Characteristics of rainstorm cloud clusters to local heavy precipitation over the eastern Qinghai-Tibet Plateau

ZHU Ping[1,2,3], LI Shengchen[3], WANG Zhenhui[1,2], XIAO Jianshe[4]

1. *Key Laboratory of Meteorological Disaster of Ministry of Education, Nanjing University of Information Science & Technology, Nanjing* 210044, *China*;
2. *School of Atmospheric Physics, Nanjing University of Information Science & Technology, Nanjing* 210044, *China*;
3. *Qinghai Province Meteorological Observatory, Xining* 810001, *China*;
4. *Qinghai Institute of Meteorological Science, Xining* 810001, *China*

Abstract: To investigate the characteristics of rainstorm clouds to local precipitation, we analyzed 19 typical cases of rainstorm process in the Eastern Qinghai-Tibetan Plateau from four hours before precipitation to two hours after based on the cloud-top t emperature data of FY-2 infrared channels. Two patterns were found, and the first was the trend of temperature at the 7 × 7 pixels region centered at automatic meteorological stations, and the second was the analysis of convection parameters through identification and tracking convective clouds. In addition, the characteristics of radar echo of rainstorm clouds were also analyzed. In this p aper, the maximum temperature gradient on cloud top is represented as G_{max}, the maximum amplitude of G_{max} within the half-hour is expressed in ΔG_{max}, and the minimum temperature on cloud top is denoted by T_{min}. We found that the variation trend of cloud-top temperature and temperature gradient at infrared channels were consistent, and the cloud-top temperature showed a decrease before increase while the temperature gradient was the opposite in precipitation stage. One or two peaks of G_{max} and ΔG_{max} happened about 0 to 11 hours earlier than the heavy precipitation. The multiple regression equation for forecasting precipitation grade was constructed by T_{min} and G_{max}. It showed that the model can well simulate the tendency of hourly precipitation and can also predict heavy rain, and the error of hourly precipitation is within one grade of precipitation. The R^2 of regression improved from 0.23 to 0.54, and the precipitation peak can be better modeled after considering the contribution of G_{max} peak. The new algorithm of clouds identification and tracking is more simple and effective than other methods. All rainstorm cloud clusters over eastern Plateau are at mid-β to mid-α scale, and their height of water vapor columns are deep but the intensity are weaker than that of the lower altitudes. The p recipitation will happen within several hours when the minimum distance between the position of clouds extremum and the meteorological station is less than 15 pixels. The rainstorm clouds have the characteristics of heavy precipitation super cell storm in r adar echo, and the extremes of T_{min} and G_{max} correspond with the extremes of vertical integrated liquid water content, echo-top height and its gradient. These results are important for identification and tracking strong convective cloud clusters and short-time precipitation forecasting in eastern Qinghai-Tibetan Plateau.

Key words: infrared channels, local rainstorms cloud clusters, identification and tracking, short-time precipitation forecasting

CLC number: P457.6 **Document code:** A

Citation format: **Zhu P, Li S C, Wang Z H and Xiao J S. 2014. Characteristics of rainstorm cloud clusters to local heavy precipitation over the eastern Qinghai-Tibet Plateau. Journal of R emote Sensing, 1 8(2): 405 – 431 [DOI: 10.11834/jrs.20143069]**

1 INTRODUCTION

Since October 19, 2004, three Geostationary Operational Meteorological Satellites were successfully launched including the FY-2C, FY-2D and FY-2E. These satellites have five spectral channels, such as infrared channel 1 (IR1, 10.3—11.3 μm), i nfrared channel 2 (IR2, 11.5—12.5 μm), infrared channel 3 (water vapor or IR3, 6.2—7.6 μm), short wave infrared channel (3.5—4.0 μm) and the visible light channel (0.55—0.9 μm). Each channel has a different resolution. Infrared radiant information can be acquired from infrared channel that comes from r eflection of cloud and ground surface at day and night. The d istribution of water vapor at the middle and upper levels of a tmosphere can be measured from IR3. Many meteorological i mages and operational products can be obtained from Satellite channels. Presently, estimation precipitation using cloud information from different channels is widespread. Adler and Negri (1988) proposed an one-dimensional cloud model to estimate the tropical precipitation of convective cloud and stratiform cloud. Vicente, et al. (1998) developed a fully automatic satellite rainfall estimation technique. The GMS-5 infrared cloud imagery

Received: 2013-04-12; **Accepted:** 2013-08-16; **Version of record first published:** 2013-08-25

Foundation: Qinghai province Science and Technology Department Project (No. 2011-Z-712); Meteorology Public Welfare Scientific Research Project (No. GYHY201306006)

First author biography: ZHU Ping (1980—), female, Ph. D. candidate, she majors in atmospheric remote sensing and weather nowcasting. E-mail: ping_xjs2010@126.com

for r aining seasons in 1998 and 1999 were used to study the relationship between brightness temperature and surface rain rates, and the result showed that heavy precipitation will occur with the decrease of brightness temperature and increase of rainfall intensity (Lin, et al, 2003). Hong, et al. (2004) employed Precipitation Estimation from Remotely Sensed Information using Artificial Neural Networks (PERSIANN) to estimate rainfall. This system extracts regional and local cloudy characteristics to evaluate d istribution of rainfall from infrared (10.7 μm) geostationary s atellite imagery at every 30 minutes. The correlation coefficient between hourly rainfall distribution and gauge rainfall measurements is 0.45. Bergès, et al. (2009) proposed a new index relies on image processing method uses cloud growing rate to estimate rainfall, which is more efficient compared with cooling index to recognize precipitation cell. The daily inspection result will be improved if use this index to estimate rainfall in large scale. The Link-based Cluster Ensemble (LCE) method is applied to a High Resolution Satellite Precipitation Estimation (HSPE) algorithm which is a modified method from the PERSIANN-CCS algorithm. The results showed that the performance of rainfall estimates improved by using the LCE compared with the Self Organizing Map (SOM) of HSPE algorithm. The LCE method can improve the Heidke Skill Score (HSS) about 5% to 7% at medium and high level of rainfall, and enhance Equitable Threat Score (ETS) by about 5% for the winter season (Mahrooghy, et al., 2011, 2012). The precipitation intensity of convective clouds in weak rainfall region is positively correlated to top temperature gradients (G) of clouds, but the corresponding G decreases in the heavy rainfall region (Lu & Wu, 1997). The intensity of convective clouds over the Tibetan Plateau was divided into four levels according to cloud top temperature: the general convective cloud (Ⅰ, −32— −54℃), the strong convective cloud with thunderstorm(Ⅱ, −54— −64℃), the stronger convective cloud through the troposphere top(Ⅲ, −64— −80℃), the strongest convective cloud(Ⅳ, ≤ −80℃). Previous results showed that the top brightness temperature is mostly between −32℃ and −54℃ over the Tibetan Plateau (Jiang & Fan, 2002). The possible precipitation intensity and distribution of clouds in one hour were estimated based on the movement of area with the largest temperature g radient around the strong low-temperature center of cloud clusters (Hu, et al., 2005). The large brightness temperature gradient region on cloud top is easy-happening area of disastrous weather (Zheng & Xi, 2006). Tropical Cyclone (TC) intensity is negatively correlated with the cloud-top brightness temperature (TBB) (Chen, et al., 2006). Rainfall intensity of hourly precipitation gradually increases and probability of heavy rainfall distinctly rises with the decrease in TBB on cloud top (Teng, et al., 2006). The precipitation intensity of correspondent station is large when the TBB rapidly rose from the lowest temperature value and rainfall appeared in the area of great temperature g radient (Zhang, et al., 2007). The time and the region of heavy rainfall correspond to the time and the center of low TBB, and the precipitation intensity has a better relation with TBB of a s ingle station (Zhao & Cheng, 2009). Identification rainstorm clouds was implemented by computation the Deep Convective Index (DCI) and brightness temperature difference at infrared channels, and the development of convective cloud and the o ccurrence of severe convection are connected (Li, et al., 2010. Hu & Li, 2012). Short-time prediction to severe convective clouds is realized based on TBB and TBB threshold of infrared images. The average TBB and the minimum TBB on cloud top both have better relations with the hourly precipitation measured at precipitation station (Liu, et al., 2012).

The active convection has notably enhanced in summer and short-time heavy rainfall is abnormally frequent because of the extreme weather events increasing in recent years in arid and semi-arid district in the east of Qinghai-Tibet Plateau. The extreme weather events lead to disasters of mountain torrents which caused great economic losses. The topography has a great influence on convectional precipitation and the precipitation is unevenly distributed because of great terrain fluctuations. H owever, there are only two Doppler radars to monitor and warn the strong convective weather in the east of Plateau, so its detection scope is limited at present. Numerical forecasting models are inapplicable to local convective precipitation, and the south Plateau is covered with cloud all the year around. Therefore, we a nalyze the local rainstorm processes in the eastern Plateau based on the FY-2 data at infrared channels to study the relationships between cloud parameters and hourly precipitation, and we aim to improve the forecasting precision for short-time heavy rainfall to reduce the losses caused by disastrous weathers.

2 DATA

In this paper, 19 typical cases were used in the eastern parts of Qinghai-Tibet plateau during 2005—2010. The dataset is i llustrated in Table 1. The form of the beginning and ending time of precipitation is year-month-date-hour. For example, the beginning and ending time of precipitation in case 1 is August 14, 2005 18:00 to August 15, 2005 6:00. The time in the OHP_{max} column is the time of OHP_{max} measured at automatic meteorological stations. There are 13 automatic meteorological stations in the eastern Plateau, each country has only one automatic meteorological s tation. The range from Jianzhan to Hualong site has the smallest distance (only 30 km) of inter-site, which is shown in Fig. 1. The

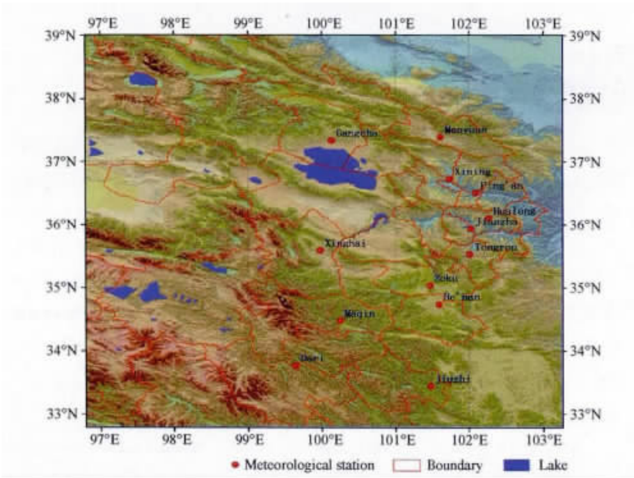

Fig. 1 The distribution map of automatic station for the typical rainstorm processes in the eastern Qinghai-Tibet Plateau

Table 1 The local rainstorm processes in the eastern Qinghai-Tibetan plateau (Beijing time)

Case number	Station number	Station name	The beginning and ending time of precipitation	OHP_{max} (mm) /time
1	56043	Maqing	2005-08 1418-1506	27.0/24:00
2	56046	Dari	2006-07 1210-1216	25.0/16:00
3	56067	Jiuzhi	2006-07 2020-2107	27.5/02:00
4	56065	He´nan	2007-07 1616-1622	25.1/22:00
5	52765	Menyuan	2007-08 0713-0720	28.0/19:00
6	52754	Gangcha	2007-08 2014-2101	33.0/20:00
7	52866	Xining	2007-08 2514-2606	28.0/22:00
8	52943	Xinhai	2008-07 2811-2823	25.8/17:00
9	56065	He´nan	2009-07 1513-1522	32.7/19:00
10	52963	Jianzha	2009-08 0214-0308	27.1/01:00
11	52943	Xinhai	2009-08 2412-2505	27.5/18:00
12	52963	Jianzha	2010-05 2819-2902	25.1/01:00
13	52875	Ping´an	2010-08 0711-0718	25.0/17:00
14	52968	Zeku	2010-08 1013-1100	27.3/19:00
15	52968	Zeku	2006-07 2112-2121	29.1/18:00
16	52765	Menyuan	2006-09 0315-0401	26.1/21:00
17	56065	He´nan	2009-07 2011-2018	49.1/17:00
18	52877	Hualong	2010-08 0711-0719	25.1/17:00
19	52974	Tongren	2010-09 2015-2102	36.6/21:00

actual data of precipitation observation was collected from Qinghai Province meteorological observatory. The FY-2C and FY-2E data in the format of HDF5 were provided by National Satellite Meteorology Center. By extracting gray values at infrared channels and correspondent calibration tables within four provinces (72.89°E—108.73°E, 25.74°N—50.60°N) including Qinghai province, we can get the cloud-top brightness temperature or black body temperature. The resolution of image is 0 .05° per pixel, which approximately equals to 5 km per pixel.

3 THE VARIATION CHARACTERISTICS ANALYSIS OF CLOUD-TOP TEMPERATURE WITHIN THE LIMITED REGION

As shown in Fig. 1, there are large topography fluctuations and occupied land in the east plateau, and automatic meteorological stations are mostly located in valley. The smallest distance is larger than the average range of automatic meteorological s tations in mountains of our entire country. We choose the r ectangular region of 35 km × 35 km (Fig. 2) centered at meteorological stations as research region to analyze the relationship b etween precipitation and changing of convective cloud over s tation, according to the diameter of meso-miso-scale severe c onvective cloud nucleus which is about 10—20 km. The inter-site distance of automatic meteorological station in cure region of nationwide mountain flashflood disaster which is about 20—4 0 km, and the average inter-site distance in mountain area. In this paper, the rectangular region of $M \times N$ pixels consists of 7 × 7 pixels, and each block expresses a pixel. The black block is the place of rainstorm station as shown in Fig. 2.

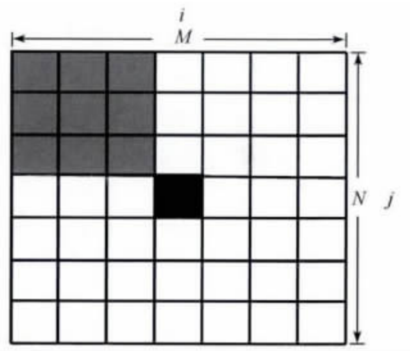

Fig. 2 The diagram of computing region centered around rainstorm station

Previous studies (Lu & Wu, 1997; Zheng & Xi, 2006; Teng, e t al., 2006; Zhang, et al., 2007; Zhao & Chen, 2009) have shown that cloud-top temperature gradient and minimum temperature both have preferably correspondent relationships with p recipitation. The decrease of cloud-top temperature indicates the increase of cloud-top height and the development of cumulus, and vice versa. Likewise, the cloud-top temperature gradient i ndicates the changing of cumulus which reflects the transformation of inhomogeneity of local temperature distribution on cloud top. Aimed at the cloud block in the studied region, the multi-time images data at infrared channels from four hours ahead of precipitation to two hours after in Table 1 were selected to c ompute the minimum cloud-top temperature (i. e. T_{min}) and the maximum temperature gradient (i. e. G_{max}).

The cloud-top temperature gradient (i. e. G) is obtained in 3 × 3 windows as the gray region shown in Fig. 3 and defined as Eq. (1).

$$G = \sqrt{[T(i+1,j) - T(i-1,j)]^2 + [T(i,j+1) - T(i,j-1)]^2} \quad (1)$$

where i and j are the coordinate of pixel, T is cloud-top temperature (unit is ℃, $T = TBB - 273.16$). Compute G of each 3×3 window in 7×7 rectangular region as shown in Fig. 2, so get the G_{max}.

3.1 Analyses on the temperature extremum and its lead-time

The extremum of cloud-top temperature and lead-time (t_{ohpmax}) of the measurement time on integral hour of hourly maximum precipitation were analyzed in Table 1, and the maximum climbing amplitude of G_{max} within half-hour is expressed in ΔG_{max}. Since G_{max} and ΔG_{max} has 1—2 peak values in rainfall process, the calculated value from IR1 is listed. $t_{\Delta G max}$, t_{1Gmax}, t_{2Gmax} and t_{Tmin} respectively means the lead-time of ΔG_{max}, the first peak of G_{max} (i.e. G_{1max}), the second peak of G_{max} (i.e. G_{2max}) and the minimum vale of T_{min} to t_{ohpmax}. As shown in Table 2, the blank space means no G_{2max}. The time range of $t_{\Delta G max}$, t_{1Gmax}, t_{2Gmax} and t_{Tmin} is 2—11 h, 1—10.5 h, 0—3 h and 0—10 h (case 1—15, for example) or −0.5— −2.5 h (case 16—19, for example), respectively. The extremes of ΔG_{max}, G_{1max}, G_{2max} and T_{min} are 3.4—22.3℃, 13.2—48.3℃, 16.4—51.2℃ and −40.6— −90.3℃, respectively, where the T_{min} values are belonged to the grade of the strongest convective cloud (Jiang & Fan, 2002), for example, in case 3, case 14, case 15 and case 17, all the T_{min} extremes are less than −80℃. In Table 2, there are 15 cases appeared G_{2max} before the strongest hourly precipitation ending, and 12 cases appeared $t_{2Gmax} > 0$, 14 cases $t_{\Delta G max} > t_{2Gmax}$, 10 cases $t_{\Delta G max} > t_{1Gmax}$. In the other four cases, there is only one peak of G_{max} before the strongest hourly precipitation ending, where 3 cases happened $\Delta G_{max} < 8$℃ and $t_{Tmin} > 1$ h, including one case with $G_{1max} > 30$℃ and T_{min} equal to −43℃, and two cases with $G_{1max} > 13$℃ and T_{min} equal to −82.3℃. There is only one case with $\Delta G_{max} > 8$℃ and $G_{1max} > 40$℃. In all 19 cases except case 10 in Table 2, there are some correspondent relations of precipitation to cloud-top temperature, such as the heavy precipitation occurs within three hours when $G_{2max} > 15$℃, or within six hours when $\Delta G_{max} > 8$℃ & $G_{1max} > 15$℃, or $G_{1max} > 30$℃, or $T_{min} < -60$℃.

Table 2 shows that all G_{max} peaks appear before the strongest hourly precipitation ending in the 19 cases, and the T_{min} values occur before the ending in case 1 to case 15 and after the ending in case 16 to case 19. Table 2 indicates that the strongest rainfall probably happens before the highest cloud-top or after, but certainly after the biggest height gradient of cloud-top (means the maximum G_{max}). The exact precipitation time and rain intensity are determined by the specific configuration of heat, dynamic and moisture condition required for rain.

Table 2 Cloud-top temperature extremum and its lead-time of 19 rainstorm processes in the eastern Qinghai-Tibetan Plateau

Case number	$t_{\Delta G max}$/h	ΔG_{max}/(℃/0.5 h)	t_{1Gmax}/h	G_{1max}/℃	t_{2Gmax}/h	G_{2max}/℃	t_{Tmin}/h	T_{min}/℃	T_{min} grade
1	7.0	12.7	5.5	27.4	3.0	16.4	5.0	-53.3	Ⅰ
2	2.5	13.1	1.0	46.1	—	—	1.0	-49.8	Ⅰ
3	2.5	3.4	2.5	16.4	—	—	1.5	-82.3	Ⅳ
4	5.5	15.4	5.0	31.2	0.5	19.5	3.5	-74.3	Ⅲ
5	5.0	8.2	3.5	25.1	0	20.1	0.5	-50.7	Ⅰ
6	2.0	19.3	2.0	28.0	1.0	33.3	0.5	-40.6	Ⅰ
7	2.0	8.2	4.0	20.1	2.0	24.8	0	-59.7	Ⅱ
8	4.0	13.5	4.0	29.1	1.5	29.2	1.5	-62.9	Ⅱ
9	4.0	14.1	3.5	28.9	1.5	33.7	1.5	-69.0	Ⅲ
10	11.0	4.1	10.5	13.2	—	—	10.0	-43.0	Ⅰ
11	3.0	22.3	3.0	37.4	1.0	44.7	1.0	-62.6	Ⅱ
12	2.5	8.2	3.5	16.4	1.5	27.0	4.0	-60.5	Ⅱ
13	2.5	19.4	2.5	35.6	1.0	44.3	0.0	-69.5	Ⅲ
14	4.0	13.6	4.0	42.2	2.5	43.2	1.5	-84.6	Ⅳ
15	3.0	10.8	2.5	38.5	1.0	30.1	0.5	-90.3	Ⅳ
16	2.0	9.0	2.0	22.8	0	30.2	-2.0	-69.8	Ⅲ
17	2.0	15.4	1.5	33.7	0	39.6	-2.5	-85.4	Ⅳ
18	2.5	19.8	2.0	48.3	1.0	51.2	-2.0	-69.1	Ⅲ
19	3.0	6.4	1.0	32.2	—	—	-0.5	-60.3	Ⅱ

3.2 Analysis on the variation trends of cloud-top temperature

Take the rainstorm processes of Maqin on August 14, 2005 and Tongren on September 20, 2010 as examples. The two cases respectively indicate the variation trends of cloud-top temperature for T_{min} value before and after the strongest hourly precipitation ending. As shown in Fig. 3 and Fig. 4, the variation trend of T_{min} at infrared channels is approximately concordant, so is G_{max}. The cloud-top temperature values of IR1 and IR2 remain close proximity to each other. The values of cloud-top temperature of IR1 and IR2 may be positive or negative, while the temperature of IR3 keeps less than −20℃ throughout the precipitation process which indicates that the deep water-vapor columns has arrived at the middle and upper level of troposphere. Before the beginning of precipitation (denoted by negative column on the left side of Fig. 3 and Fig. 4), cloud-top temperature gradually falls with the development of cumulus and the rising of cloud top. While there is still a pause in the development process of cumulus, which shows a little increase of cloud-top temperature and a decrease of temperature gradient (Fig. 3 and Fig. 4). The cumulus approximately continue to development (Fig. 4). During the precipitation stage, the hourly precipitation greater than or equal to 0.0 is denoted by positive column. The measuring time of the first hourly precipitation is at 18:00 (Fig. 3), and at 15:00 (Fig. 4). Cloud-top temperature increases within the first hour of precipitation because the latent heat r eleased by precipitation incireased the atmospheric temperature. Then cumulus top temperature ascends first and then descends, and cumulus is gradually weakening. After the precipitation ending, the cloud-top temperature gradually returns to a balanceable state with the atmosphere. In addition, there are two decreases in the rising process of T_{min} which indicates the short-time development of cumulus in the decreasing process of cumulus-top height (Fig. 3). The large G_{max} corresponds to the big slope of T_{min} curve (Fig. 3 and Fig. 4), which is shown d uring 17:00 to 19:30, 19:30 to 00:30 in Fig. 3, and 17:30 to 2 3:00 in Fig. 4.

The general variation trend of cloud-top temperature is o btained through selecting the appropriate precipitation period according to precipitation time. As shown in Fig. 5, where the three hours before precipitation is represented by $t-$ in the horizontal axis, and the correspondent hourly precipitation by negative column, and the ending time of the strongest hourly precipitation is denoted by t. The six hours in precipitation stage are respectively expressed by $t-1$, $t-2$, $t-3$, $t+1$, $t+2$, $t+3$, and the hourly precipitations are expressed in columns of greater than or equal to zero. The two hours after precipitation ending are i ndicated by $t--$. The variation trends of cloud-top temperature of IR1, IR2 and IR3 are consistent, and that of temperature gradient is the same, where the temperature curve of IR1 is close to IR2. The cloud-top temperature of IR3 is below −20 ℃ from $t-$ to $t--$. The G_{max} peak appears in the period from $t-3$ to t. The temperature curve shows a decrease before increase, and the t emperature gradient is the opposite in the precipitation stage. After the precipitation ending, cloud-top temperature gradually returns to the atmospheric temperature. In the process of case 1 to case 15 in Table 1, the temperature curve has a little decrease at first and then increase. For example, the temperature of IR1 is −67.17℃, −66.63℃, and −68.41℃ in time sequence, the minimum temperature occurs at $t-1$ and its temperature gradient is the largest. In the process of case 16 to case 19, cloud-top temperature gradually drops within the three hours before t. The maximum temperature gradient occurs at t time, and the minimum temperature at $t+2$, which means the cumulus-top r eaches the greatest height in the meantime.

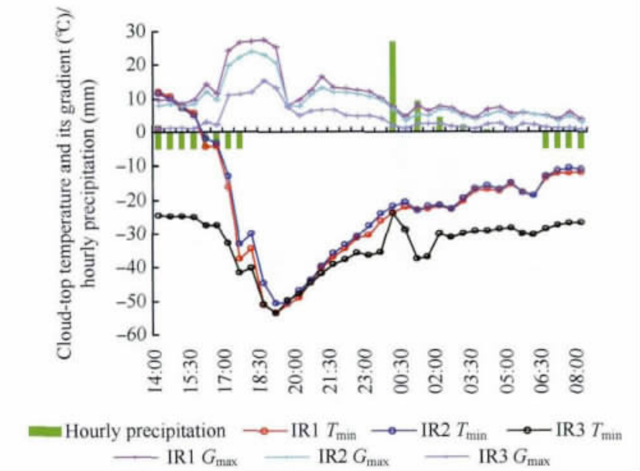

Fig. 3 Variation trends of cloud-top temperature on August 14, 2005 over Maqing station

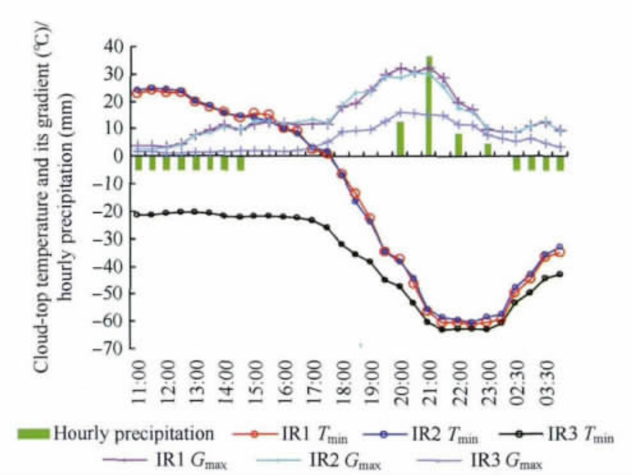

Fig. 4 Variation trends of cloud-top temperature on September 20, 2010 over Tongren station

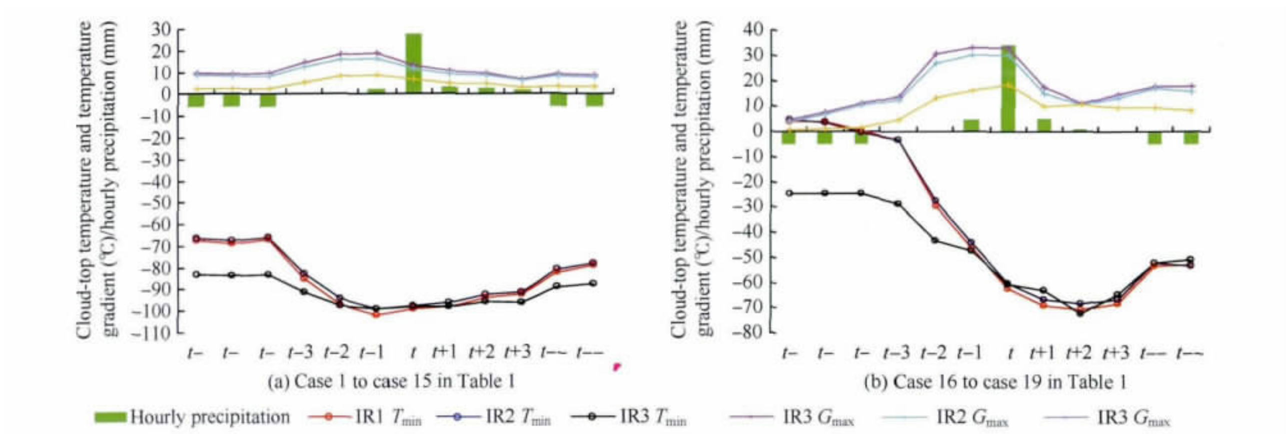

Fig. 5 The general variation trends of cloud-top temperature of the 19 typically local rainstorm processes in the eastern Qinghai-Tibetan Plateau

3.3 Forecast equation for hourly precipitation grade and error check

According to the analysis above, we constructed multiple regression equation to forecast precipitation grade referring to the standard of short-time precipitation intensity in Qinghai province (Zhu, et al., 2012), such as general precipitation (grade Ⅲ, 0 mm ≤ y < 8 mm), short-time sever precipitation (grade Ⅱ, 8 mm ≤ y < 16 mm), short-time rainstorm (grade Ⅰ, y ≥ 16 mm). The T_{min} of IR1 and IR3 (denoted by x_1 and x_2 respectively) and the G_{max} of IR1 (denoted by x_3) are chosen as independent variables, and the hourly precipitation as dependent variable (denoted by y). Based on the 62 times of $y > 1$ mm, the multiple regression equation is constructed as

$$y = 0.61 + 0.01x_1 - 0.11x_2 + 0.45x_3 \quad (2)$$

This equation passes the test of $P < 0.01$ (i. e. the test differences are significant), the R^2 is equal to 0.23 which can only explain 23% variance of dependent variation.

Since the x_3 peak always occurs before the strongest hourly precipitation ending, indicating that the x_3 peak may have important contribution to hourly precipitation, and the stepwise regression equation based on x_3 peak is constructed as

$$y = -2.58 + 1.03x_3 - 0.01{x_3}^2 \quad (3)$$

The dependence reliability is at least 99% (i. e. $P < 0.01$), the R^2 is equal to 0.55. Take the contribution of x_3 peak to precipitation peak into consideration, the multiple regression equation is c onstructed as

$$y = -2.09 + 0.12x_1 - 0.16x_2 + 0.65x_3 \quad (4)$$

Eq. (4) passes the significant test ($P < 0.01$), the R^2 improved to 0 .54, which can better simulate the trend of hourly precipitation with cloud-top temperature variation.

To test the forecasting effect of Eq. (2) to Eq. (4), we suppose the ending time of the strongest hourly precipitation is still denoted by t, and the precipitation periods are selected from $t-1$ to $t+3$ based on the actually measuring time of hourly precipitation. The test is divided into two cases, nonuse and use the x_3 peak at t time for the true value of independent variation x_1 to x_3. In Fig. 6, the legend of "$R^2 = 0.23$", "$R^2 = 0.55$" and "$R^2 = 0.54$" respectively stands for Eq. (2), Eq. (3) and Eq. (4). The simulated results of equations can primarily r eflect the trend of true value with time. The grade difference b etween the true-peak and the modeled-peak value is within one grade. The result of nonuse the x_3 peak can predict strong precipitation one hour ahead of time. While the result of using the x_3 peak is distinctively close to the truth, but the lead time is within 0. 5 hour. In general, the equations denoted by $R^2 = 0.55$ and $R^2 = 0.54$ have both considered the x_3 peak contribution to strong precipitation, and its modeled values are more close to the truth. So, G_{max} and G_{max} peaks make an important contribution to hourly precipitation and precipitation peak.

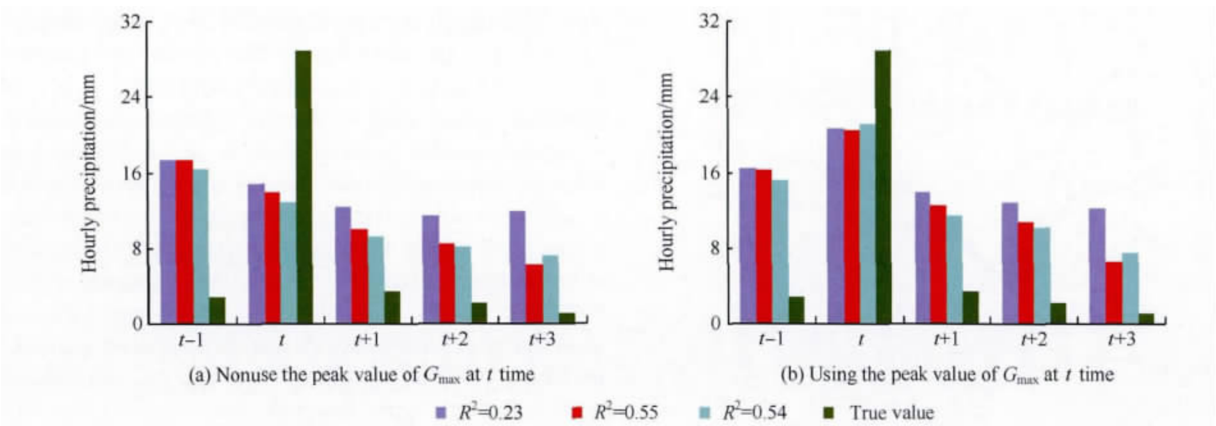

Fig. 6 Comparison chart of hourly precipitation grade of local rainstorm process

Additionally, the statistical analysis on the minimum cloud-top temperature and the maximum temperature gradient of the 19 cases within three hours before the beginning of precipitation has shown that x_1 is in the range of 8.6℃ to −74.7℃, x_2 is −21.8℃ to 68.7℃, and x_3 is 4.1℃ to 40.6℃. There are only two cases (including case 5 and case 6) where x_1 is greater than 0 ℃. So the preliminary condition of immediate precipitation may simultaneously met the conditions, $x_1 < 0$℃, $x_2 < -20$℃ and $x_3 > 4$℃.

4 CONVECTIVE CLOUDS AND PRECIPITATION AT METEOROLOGICAL STATION

4.1 The identification and tracking of convective clouds

For the continues cloud images, we selected the temperature threshold (Jiang & Fan, 2002) which is denoted by T_C, and e xtracted its contour. Based on the threshold, we computed the number of pixels within the contour. If the number is greater than or equal to 100, then the image within the contour is c onvective cloud. Then calculate the correlation coefficients of convective clouds with the distance between centroid less than 100 km. The greatest matchable cloud cluster must have the m inimum centroid distance and the maximum correlation coefficient.

Step 1 Extract the contour of cloud cluster based on T_C as −32℃, and compute the total number (n_c) of pixel within the contour. If n_c is greater than or equal to 100, the cloud within the contour is general convective cloud cluster (Jiang & Fan, 2002). Then continue to calculate its minimum temperature (T_{min}). If T_{min} is less than or equal to −80℃, extract contour based on T_C as −54℃ and compute n_c again. If n_c is still greater than or equal to 100 (Liu, et al., 2012), the cloud within the contour is believed to be the strong convective cloud (Jiang & Fan, 2002), and then calculate its area and record its code number.

In Table 1, the rainstrom cloud clusters are all belonged to mid-β to mid-α scale with their areas in 2600 km^2 to 1100000 km^2. Among those, several times of convective clouds are at mid-α scale in the rainstorm process of Xinghai station on July 28, 2008 (case 8 in Table 1). For example, on July 12, 2006 (case 2 in Table 1), T_C is equal to −32℃. And the total number of c onvective clouds in four provinces (72.89—108.73°E,2 5.74—50.60°N) from 14:30 to 16:00 is 18, 18, 14 and 18, r espectively. In this period, the clouds over Dari station is general convective cloud, and its contour is respectively represented by blue, amethyst, green and rose lines as shown in Fig. 7 (red lines denote the boundary of Qinghai province). The clouds area is mid-β scale and gradually increases from 3986.6 km^2 to 77059.1 km^2 while the $T_{\min}$ gradually decreases from −48.2℃ to −66.4℃ within the period of 14:30 to 16:00. Consequently, the sever p recipitation at Dari station occurs within 15:00 to 16:00.

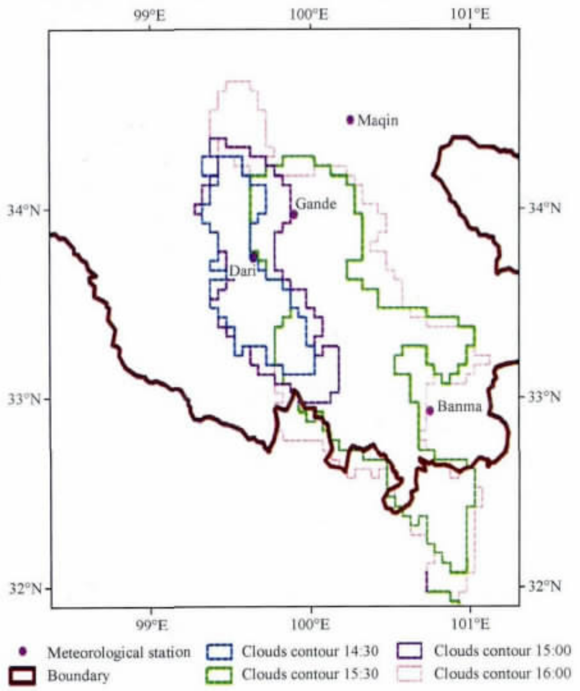

Fig.7 Contours of convective cloud clusters from 14:30 to 16:00 in Dari rainstorm process on July 12, 2006

Step 2 Calculate the centroid position(X_{CG}, Y_{CG}) and c orrelation coefficient(r) of continues cloud images. The formula of centroid position is defined as

$$X_{CG} = \frac{\sum_{i=1}^{N_P} X_i T_i}{\sum_{i=1}^{N_P} T_i} \qquad Y_{CG} = \frac{\sum_{i=1}^{N_P} Y_i T_i}{\sum_{i=1}^{N_P} T_i} \tag{5}$$

where T_i is the temperature of pixel. Suppose T_i is equal to zero when T_i is greater than −32℃. N_P is the total pixel number of convective cloud, X_i and Y_i represent longitude and latitude of pixel. The formula of correlation coefficient is defined as

$$r = \frac{\sum_{j=1}^{m}\sum_{i=1}^{n}\left(T_f(i,j) - \overline{T}_f\right)\left(T_g(i,j) - \overline{T}_g\right)}{\sqrt{\sum_{j=1}^{m}\sum_{i=1}^{n}\left(T_f(i,j) - \overline{T}_f\right)^2}\sqrt{\sum_{j=1}^{m}\sum_{i=1}^{n}\left(T_g(i,j) - \overline{T}_g\right)^2}} \tag{6}$$

where $\overline{T}_f$ is the average cloud-top temperature of cloud f, $\overline{T}_g$ is the average cloud-top temperature of the assumed cloud g. Take the cloud centroid as center point, and the pixel number at longitude and latitude direction of rectangle covered clouds is e xpressed by m and n, respectively.

Statistics on the greatest matchable convective cloud show that the moving distance is less than 100 km and the correlation coefficient is greater than 0.5, which is based on the position of cloud centroid. For instance, tracking the convective cloud cluster within the regions of four provinces on July 12, 2006, the correlation coefficient and distance between the cloud 0 at 14:00 and the cloud 0 to 18 at 14:30 are shown as Table 3. The results show that the greatest machable cloud cluster with cloud 0 at 1 4:00 is just the cloud 0 at 14:30, and the correlation coefficient is 0.9 and the distance between centroids is 21.2 km.

Table 3 Computation values of cloud 0 to cloud 18 at 14:30 in Dari rainstorm process on July 12, 2006

Clouds code	Correlation coefficient	Centroid distance/km
0	0.9	21.2
1	0.6	1573.0
2	0.7	1181.4
3	0.7	1039.5
4	0.6	1041.1
5	0.5	1025.1
6	0.7	1909.7
7	-0.4	2483.1
8	0.6	2213.4
9	0.6	2406.4
10	0.3	2203.2
11	0.6	2560.1
12	0.6	2966.1
13	0.6	2621.9
14	0.6	2615.7
15	0.6	2665.0
16	0.6	2729.3
17	0.6	2742.6
18	0.0	2970.6

Step 3 Let the centroid of cloud 0 at t_0 be $CG_0^{t_0}$, then search the centroid ($CG_k^{t_1}$) of each clouds at t_1 image, seeking clouds with distance ($\triangle L$) between $CG_k^{t_1}$ and $CG_0^{t_0}$ less than 1 00 km. The value of m and n is based on the smaller cloud of $CG_0^{t_0}$ or $CG_k^{t_1}$ cloud when computing its correlation coefficient. The greatest matchable cloud of cloud 0 at t_0 must be the cloud with the largest correlation coefficient and the minimum distance of $\triangle L$ is less than 100 km.

Likewise, the greatest matchable cloud of cloud 1, 2, 3, …, 18 at t_0 can be obtained at t_1 image.

The method of identification and tracking convective clouds can be used more simply with smaller computation complexity and the high accuracy.

4.2 Verification of identification and tracking

The effect of identification and tracking convective clouds on August 10, 2010 is shown in Fig. 8 and Table 4. The colored clouds are identified. The correlation coefficients are computed with identified clouds and tracked clouds in adjacent time in Table 4. From 13:00 to 16:00, the colored clouds belong to the general convective clouds because the T_{min} is within the range of 220.7—196.2 K (i. e. −52.3— −76.8℃). From 15:30 to 16:30, the clouds within dotted line are also identified, its calculated values are shown as the shaded values in Table 4. Taking the clouds marked centroid point as example, the clouds from 13:00 to16:00 are respectively accordant convective cloud of identification and tracking as shown in Fig. 8(a) to Fig. 8(g). There is no tracking result at 16:30, and the identified convective cloud 22 is near to Zeku station as shown in Fig. 8(h). The colored cloud 6 at 13:30 is just the greatest matchable cloud of the colored cloud 6 at 13:00, and the maximum correlation coefficient is 0.7 with the distance between centroid of 36.2 km. The area of colored clouds reaches at mid-β scale from 15:30. The cloud 15 within dotted line at 15:30 in Fig. 8(f) matches the cloud 17 at 16:00 in F ig. 8(g), whose correlation coefficient is 0.9, and the distance between centroid is 21.8 km. The colored cloud and the cloud within dotted contour gradually combine since 15:30, until 16:30, they combine into cloud 22 with T_{min} equal to 190 K. It belongs to the strong convective cloud because the temperature threshold of colored cloud is −54℃, while that within dotted contour is −32℃. The correlation coefficients of clouds at 16:00 with the clouds at 16:30 are less than 0.5.

Table 4 The calculated values of identification and tracking to convective clouds in the Zeku rainstorm process on August 10, 2010

Time	Code of identified clouds	T_{min} /K	Code of tracked clouds	Correlation coeficient	Centroid distance /km
13:30	6	222.3	6	0.7	36.2
14:00	8	222.9	8	0.7	29.0
14:30	9	209.1	9	0.6	37.6
15:00	11	205.9	11	0.5	74.1
15:30	12,**15**	203.5,**198**	12	0.9,**0.4**	31.7,**243.1**
16:00	15,**17**	198.9,**196.2**	15	0.9,**0.9**	18.5,**21.8**
16:30	22	190		0.3,**0.4**	

Similarly, the identification of convective clouds and the tracking of small deformed clouds in local rainstorm process are right. However, it is invalid when tracking seriously deformed clouds, and its correlation coefficient is generally greater than 0.5.

4.3 Parameters for computing of convective clouds

Based on these findings, the region of large DCI and the band-difference distribution at infrared channels have great relationships with the development of convective cloud and the o ccurrence of strong convection (Li, et al., 2010; Hu & Li, 2012). The hourly precipitation at automatic rain-gauge has the same with the average temperature and the minimum temperature of cloud top (Liu, et al., 2012). And the region of high temperature gradient with the location of severe precipitation (Hu, et al., 2005; Zhen & Xi, 2006). To analyze the correspondent relations between above convection parameters and precipitation at meteorological station, we only choose the two periods, the three hours before precipitation, and that before severe precipitation. And it must be covered by convective clouds over the meteorological station due to the sparse meteorological station in Plateau.

(1) Radiation parameters

Radiation parameters include the average temperature ($\bar{T}$), the minimum temperature (T_{min}), the maximum temperature g radient (G_{max}), the infrared band-difference (T_{12}, T_{13}) at centroid position and the deep convection index (DCI_{NS}) of cloud top. The computation of G_{max} and centroid position is the same as Eq.(1) and Eq.(5) respectively. The infrared band-difference is defined by

$$\begin{cases} T_{12} = T_{CG1} - T_{CG2} \\ T_{13} = T_{CG1} - T_{CG3} \end{cases} \tag{7}$$

where T_{CG1}, T_{CG2} and T_{CG3} respectively refers to the cloud-top temperature of IR1, IR2 and IR3. The deep convection index is defined by

$$DCI_{NS} = \begin{cases} 250 - T_{CG} & T_{CG} < 250\ \text{K} \\ 0 & T_{CG} \geqslant 250\ \text{K} \end{cases} \tag{8}$$

where T_{CG} is cloud-top temperature at centroid position, the DCI_{NS} can indicate the developing extent of deep convection with the height of cloud top equal to or greater than 400 hPa since the atmospheric temperature near to the 400 hPa is generally about 250 K. The greater DCI_{NS} before the beginning of severe convection indicates the greater probability of strong convective cloud.

(2) Space parameters

Space parameters are the distance (Δl) of the clouds centroid of brightness temperature (X_{CG}, Y_{CG}), the clouds centroid of T_{min}, and the clouds centroid of G_{max} to the position of meteorological station, which are denoted by Δl_{CG}, $\Delta l_{T\min}$ and $\Delta l_{G\max}$, r espectively.

4.4 Data analysis and check

Take −32℃ or −54℃ as the thresholds of identification convective clouds. There were 18 rainstorm processes with convective clouds covering the meteorological station within three hours before sever precipitation except the rainstorm process of Jianzha on August 2, 2009 (case 10 in Table 1). Only three processes had convective clouds covering the meteorological s tation within three hours before the beginning of precipitation,

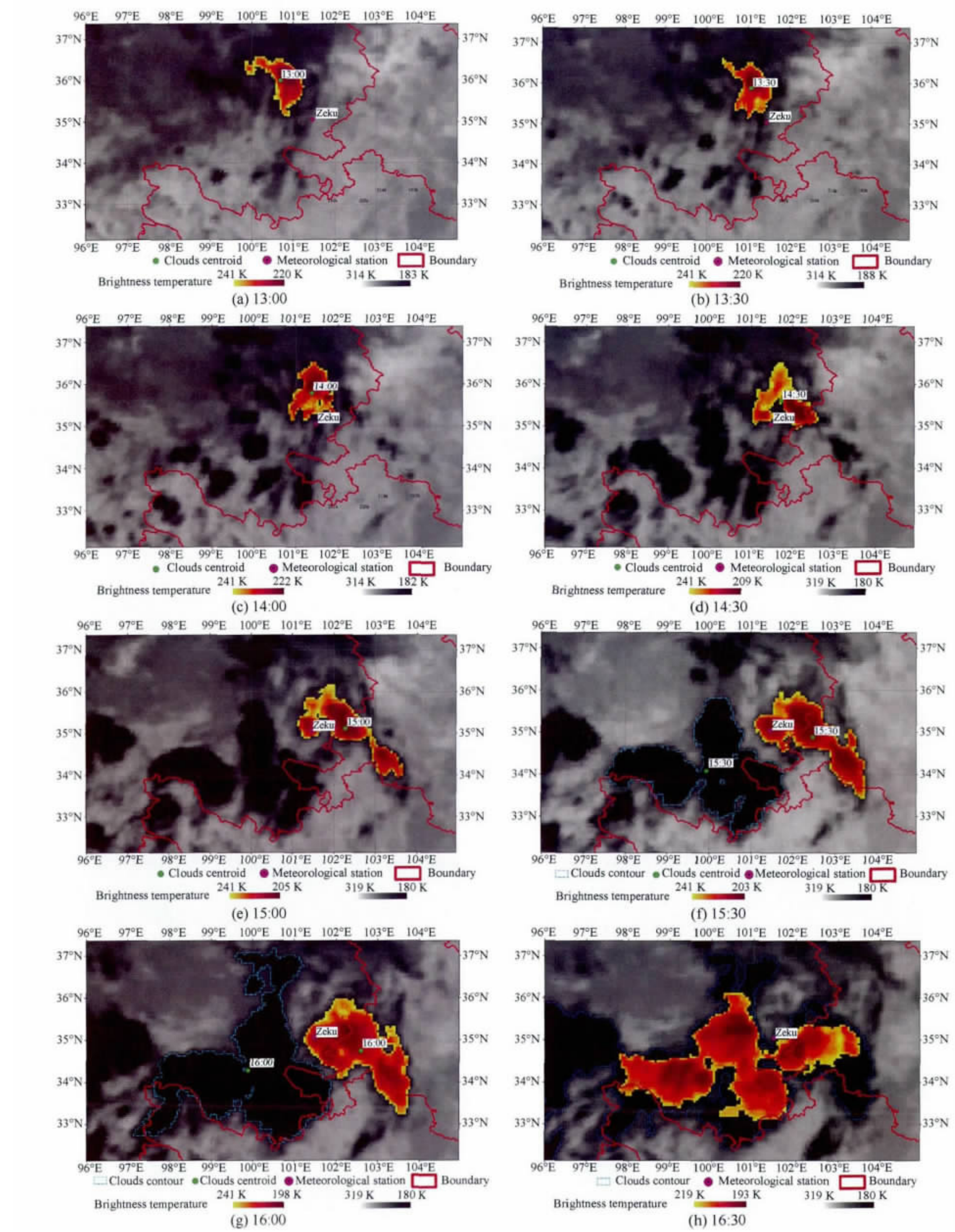

Fig. 8 The identification and tracking of convective clouds in Zeku rainstorm process on August 10, 2010

which indicate that the precipitation may appear in the condition when cloud-top temperature is higher than −32℃. However, the severe precipitation mostly occurs in less than −32℃ over plateau in summer. In the 19 typical rainstorm processes in Table 1, only one process has the thresholds of thunderstorm clouds in low elevations (Li, et al., 2010; Hu & Li, 2012) within three hours before sever precipitation, those are $T_{12} < -8$℃, $T_{13} < -10$℃ and $DCI_{NS} \geqslant 50$ in Zeku station. The 18 processes with clouds covering station have $\Delta l_{T_{\min}} > 5$ pixels, among them, 13 processes have the minimum $\Delta l \leqslant 15$ pixels. The convection parameters and the correspondently hourly maximum precipitation (i. e. OHP) with the minimum $\Delta l \leqslant 5$ pixels are listed in Table

5. t_g expresses the lead-time of the minimum Δl of convective clouds to the G_{max} in the 7×7 region over rainstorm station, t_{ohp} expresses the lead time of the minimum Δl of convective clouds to the maximum hourly precipitation ending at rainstorm station. Table 5 shows that the values of parameters have some regularities, such as the maximum $\bar{T}$ is −40℃, the minimum G_{max} is 11℃, and T_{12}, T_{13} or DCI_{NS} are all not up to the thresholds of thunderstorm clouds in low elevations. Table 5 also shows that it may be rainy or strong rainfalls when the minimum $\Delta l \leqslant 5$. The minimum Δl may be advanced or lagged by 0 to 3 h compared with the G_{max} peak, but it keeps 0.5 h to 3 h earlier than the peak of hourly precipitation.

In the rainstorm process of Maqin on August 14, 2005, the maximum OHP is 27 mm, and Δl_{Gmax} is two pixels at 22:00, and the correspondent G_{max} is 11℃ (Table 5), while the G_{max} is 13℃ within the 7×7 region centered at Maqin station at 22:00 (Fig. 9). In the rainstorm process of He´nan on July 20, 2009, the OHP is 49.1 mm, Δl_{Gmax} is three pixels at 15:30, and the correspondent G_{max} is 36℃ (Table 5), while the G_{max} is 34℃ within the 7×7 r egion centered at He´nan station at 15:30 (Fig. 10). In the rainstorm process of Dari on July 12, 2006, the OHP is about 2 5 mm, Δl_{CG} are both equal to two pixels at 14:30 and 15:00, $\bar{T}$ is respectively equal to −41℃ and −44℃, the T_{min} of convective clouds is −48℃ and −56℃ (Table 5). While the T_{min} is respectively equal to −48℃ at 14:30 and −50℃ at 15:00 within the 7×7 region centered at Dari station (Fig. 11). Obviously, the results in the limited region centered at meteorological station agree with the results of identification and tracking convective cloud clusters.

Table 5 The parameters of convective clouds with the minimum Δl equal to or less than five pixels within three hours before sever precipitation

OHP/mm	Δl_{CG}/pixel	Δl_{Gmax}/pixel	$\bar{T}$/℃	G_{max}/℃	T_{12}/K	T_{13}/K	DCI_{NS}/K	t_g/h	t_{ohp}/h
25.0	2	13	−41	36	−2	7	23	0.5	1.5
25.1	5	23	−44	29	−7	−7	33	1.5	3.0
27.0	6	2	−40	11	−2	2	13	−1.5	2.0
28.0	3	>35	−41	18	−3	0	26	−2.5	1.0
32.7	4	13	−49	39	−2	−9	34	1.0	2.5
49.1	7	3	−52	36	−2	−4	32	1.5	1.5

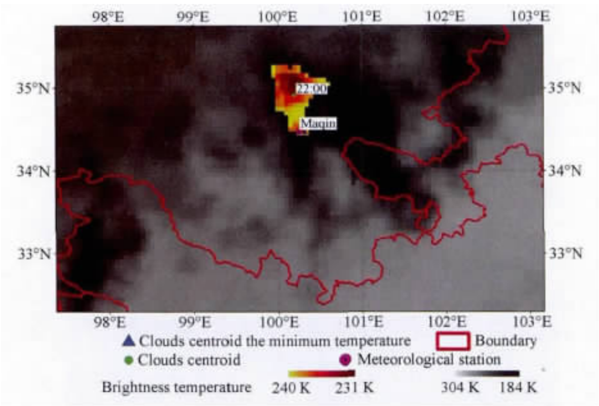

Fig. 9 Convective clouds of Maqin rainstorm process at 22:00 on August 14, 2005

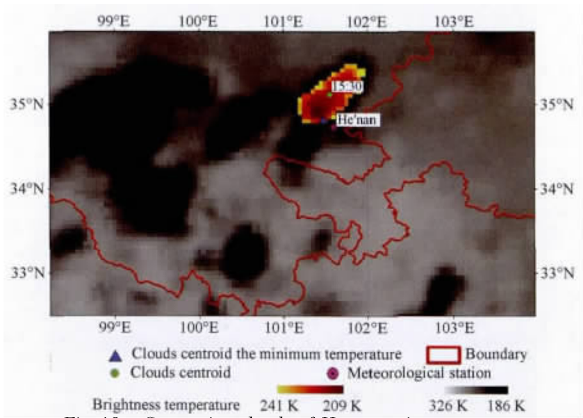

Fig. 10 Convective clouds of He´nan rainstorm process at 15:30 on July 20, 2009

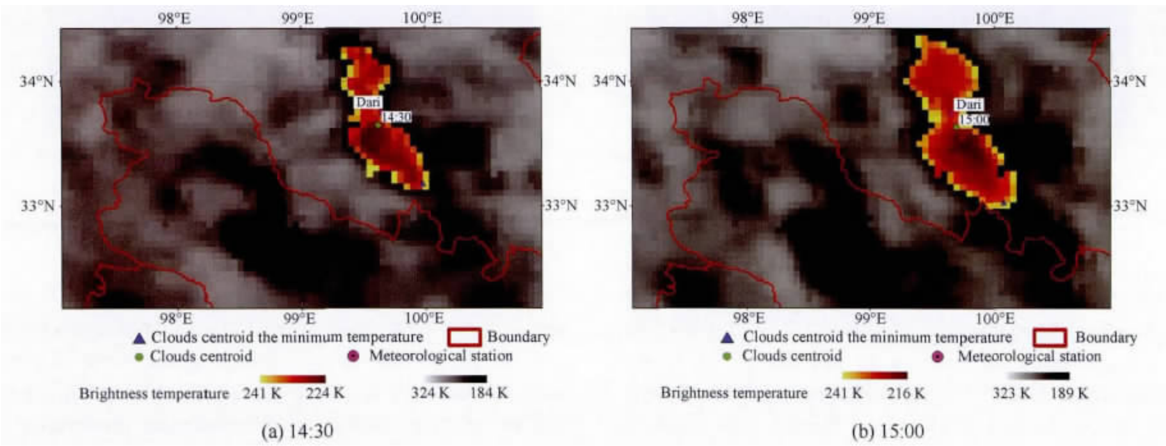

Fig. 11 Convective clouds of Dari rainstorm process on July 12, 2006

5 CHARACTERISTICS OF RADAR ECHO FOR LOCAL RAINSTORM CLOUDS

In Ping´an rainstorm process on August 7, 2010, the strongest precipitation accompaning hail, thunderbolt and gale occurred from 16:00 to 17:00, especially during 16:30 to 17:00, because the convective clouds shifted eastwards and moved northwards from Huangnan country from 14:30 gradually c ombined with clouds moved down from Haibei country from 15:00, which strengthened the combined clouds. The variation trend of cloud-top temperature in the region of 7 × 7 pixels c entered at Ping´an station is shown as Fig. 12. The T_{min} vale of IR1 and IR3 at 17:00 is equal to −69.5℃ and −60.5℃ respectively, and the G_{max} peak occurs at 16:00. The rainstorm clouds in the north of Ping´an station (Fig. 13) is cloud 7, and its space p arameters of $\Delta l_{T\min}$, Δl_{CG} and $\Delta l_{G\max}$ are respectively equal to 39, 14, 12 pixels at 16:00. The rainstorm clouds in the south of Ping´an station (Fig. 13) is cloud 18, its T_{min} of IR1 is equal to −64.2℃, and the correspondent $\Delta l_{T\min}$ is equal to six pixels at 1 6:00 when G_{max} just reaches the maximum peak. The cloud 7 has combined with cloud 18 at 16:30 with Δl greater than 30 pixels, and moved to southeast.

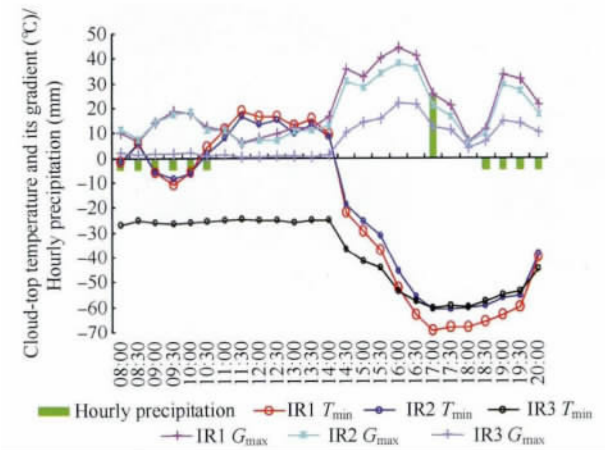

Fig. 12 Variation trend of cloud-top temperature on August 7, 2010 over Ping´an station

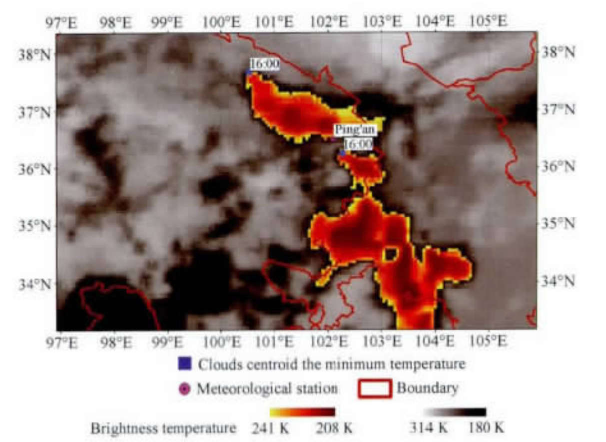

Fig. 13 Rainstorm clouds of Ping´an heavy rain process at 16:00 on August 7, 2010

From the radar echo of Ping´an heavy rain process on A ugust 7, 2010 (Fig. 14). At 16:08, the height of echo top over Ping´an station is 11 km, and the maximum height of echo top within the region of 7 × 7 pixels centered at Ping´an station is 1 5.5 km. The height gradient is large in this region which is c onsistent with the result of the maximum peak of G_{max} at 16:00 (Fig. 12). The convection over Ping´an station is strengthened at 16:30 because it is located in the combined regions of previous clouds. The front of sever convection arrives at Ping´an station at 16:32, and the maximum echo intensity reaches 66 dBz in the north of Ping´an station. The strong echo center likes a bow in the radar echo of base reflectivity factor at 2.4°elevation, as shown in Fig. 14(b). The large gradient of base reflectivity factor and the weak echo region corresponding the inflow side (as the orange arrow indicated) can be seen. From the cross section along the dotted line (Fig. 14(b)), we can approximately see the inflow at low level with the negative base velocity to the outflow at higher level with the positive base velocity (as the yellow arrow shown in Fig. 14(c)). From Fig. 14(d), we also see the weak echo region in the inflow side, the height of the strongest echo center is less than 3 km, and the height of 45 dBz echo top is greater than 6 km, which is greater than 0.5 time height of 18 dBz echo top. So the strong convective cloud belongs to super cell (Yu, et al., 2010). The storm moves toward southeast, and at 16:41, the slightly distinctive divergence downdraft emerges within the red ellipse (Fig. 14(e) and F ig. 14(f)). The obvious p ositive/negative velocity in pairsover Ping´an station means the mesocyclone wrapped in the prectpitation echo. There are two convective cells setting in the strong echo region. The position of MEHS (maximum expected hailstone diameter) equal to 5 cm is just over Ping´an station. The strong echo center of base reflectivity factor at low level makes a slight S-shape (Fig. 14(f)). B ecause there is still one inflow located in the front side of s upercell (Fig. 14(b), Fig. 14(c) and Fig. 14(f), so the strong echo has developed into the distinctively heavy precipation supercell (Yu, et al., 2010). The maximum vertical integrated liquid water c ontent reaches 62 kg/m^2 within the region of 7 × 7 pixels centered at Ping´an station at 16:48 (Fig. 14(g)), and the maximum echo intensity of convection is 65 dBz and its correspondent height is 3.9 km. The height of 30 dBz echo top of convection cell is greater than 12 km. The storm cell continues to move southeast, and until 16:55, the MEHS increases to 6 cm (as shown in Fig. 14(h)). Meanwhile, the height of echo top within this region reaches the largest height (i. e. 17.1 km) in this rainstorm process (Fig. 14(i)), which is consistent with the results that T_{min} reaches the vale at 17:00 within this region.

The analysis of other rainstorm process has the similar r esults. The moment of G_{max} peak corresponds with the maximum height gradient of 18 dBz echo top. The time of T_{min} vale at i nfrared channel 1 or channel 2 corresponds with the maximum height of 18 dBz echo top, and that at channel 3 corresponds with the maximum vertical integrated liquid water content in radar echo. The rainstorm clouds have the characteristics of heavy precipitation super cell in radar echo, such as the distinctive reflectivity gradient at low level, the weak echo region corresponding front inflow at middle-low level, and the rear-side outflow in

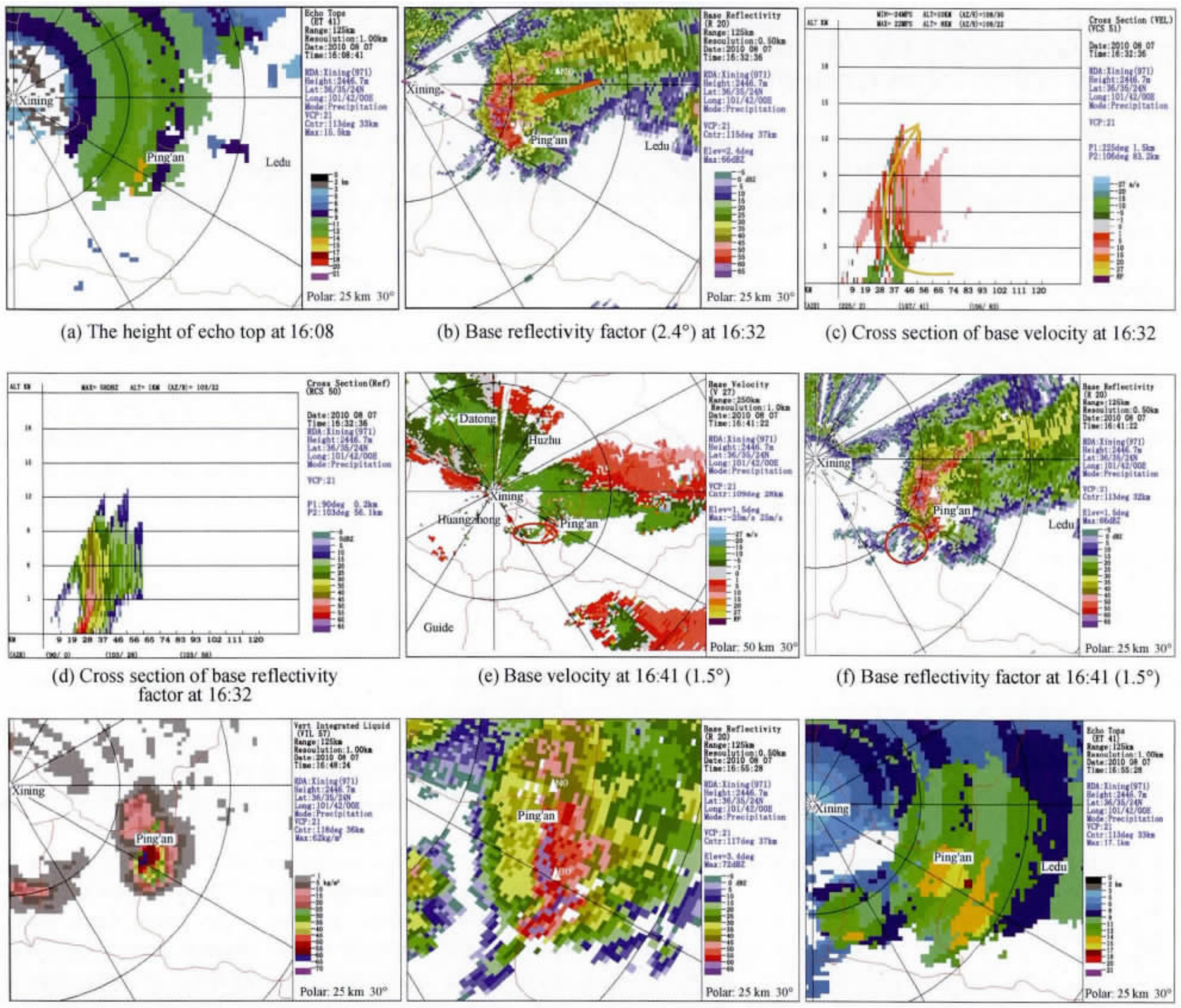

(a) The height of echo top at 16:08
(b) Base reflectivity factor (2.4°) at 16:32
(c) Cross section of base velocity at 16:32
(d) Cross section of base reflectivity factor at 16:32
(e) Base velocity at 16:41 (1.5°)
(f) Base reflectivity factor at 16:41 (1.5°)
(g) Vertical integrated liquid water content at 16:48
(h) Base reflectivity factor at 16:55 (1.5°)
(i) The height of echo top at 16:55

Fig. 14 Radar echo of local rainstorm clouds of Ping´an heavy rain process on August 7, 2010 (Volume scan every six minute)

heavy rain stage. The maximum echo intensity may excess 60 dBz and its echo top height is generally less than 3 km. The maximum vertical integrated liquid water content may reach 50 kg/m^2 or more. The height of 18 dBz echo top may grow to 15 km above the local ground surface. The height of 3 0 dBz or 45 dBz echo top is mostly greater than 0.5 time of the 18 dBz echo top height. This super cell will bring the disastrous weather such as thunderstorm, hailstone, strong winds and so on.

6 CONCLUSIONS

This paper analyzed 19 typical cases of rainstorm process in the Eastern Qinghai-Tibetan Plateau for the period of four hours ahead of precipitation to two hours after based on the cloud-top temperature data of FY-2C and FY-2E at infrared channels, and the analysis is divided into two patterns. The variation trend of cloud-top temperature with time aimed at the region of 7 × 7 pixels centered at automatic meteorological station was analyzed. Second, we identified and tracked convective cloud clusters, and computed its parameters. The results preliminarily obtain the s pecific upcoming signs of rain and the advanced time compared with precipitation and heavy precipitation. In addition, the characteristics of radar echo of rainstorm clouds are also analyzed. The maximum temperature gradient on cloud top is represented as G_{max}, the maximum amplitude of G_{max} within the half-hour is expressed in ΔG_{max}, and the minimum temperature on cloud top is denoted by T_{min}. Main results showed below.

The variation trend of cloud-top temperature and temperature gradient at infrared channels is respectively consistent. The cloud-top temperature descends at first and then ascends, the temperature gradient is the opposite in precipitation stage. One or two peaks of G_{max} and ΔG_{max} are about 0 to 11 hours earlier than the heavy precipitation. The extremes of ΔG_{max}, G_{max} and T_{min} can reaches 22.3℃, 48.3℃ and −90.3℃, respectively.

The multiple regression equations for forecasting precipitation grade are constructed by T_{min} and G_{max}, which can well simulate the tendency of hourly precipitation, and can also predict heavy rain in advance. The forecasting error of hourly precipitation is within one grade of precipitation. The R^2 of r egression improved from 0.23 to 0.54, and the precipitation peak can be better modeled after considering the contribution of G_{max} peak.

The algorithm of identification and tracking convective cloud clusters is more simple and effective than other methods. The precision of identification and tracking is 100% for the little deformed cloud clusters, which ordinarily have the correlation coefficient greater than 0.5.

All of the rainstorm cloud clusters over eastern Plateau are at mid-β to mid-α scale. Its height of water vapor columns is deep but its intensity is correspondingly weaker than lower altitudes. The precipitation will happen within several hours when the minimum distance between the position of clouds extremum and the meteorological station is less than 15 pixels.

The rainstorm clouds have the characteristics of heavy p recipitation super cell storm in radar echo. The G_{max} peak corresponds with the maximum height gradient of 18 dBz echo top. The T_{min} vale at infrared channel 1 or channel 2 corresponds with the maximum height of 18 dBz echo top, and that at channel 3 corresponds with the maximum vertical integrated liquid water content in radar echo.

The sample number is limited due to the complex topography, sparse meteorological station, uneven distribution of precipitation and the convective precipitation impact of topography and so on over the Qinghai-Tibetan Plateau, the conclusions will be continued to improve and perfect in the future work.

REFERENCES

Adler R F and Negri A J. 1988. A satellite infrared technique to estimate tropical convective and stratiform rainfall. Journal of Applied Meteorology, 27(1): 31 – 51 [DOI: 10.1175/1520 – 0450(1988)027 <0030: ASITTE>2.0.CO;2]

Bergès J C, Jobard I and Roca R. 2009. A new index to estimate precipitation using cloud growing rate. Geophysical Research Letters, 36 (8): 1 – 5 [DOI: 10.1029/2008GL036665]

Chen P Y, Duan Y H, Yu H and Hu C M. 2006. Application of equivalent black body temperature to forecast of TC intensity in Northwest Pacific. Acta Meteorologica Sinica, 64(4): 474 – 484

Hong Y, Kuo L H, Sorooshian S and Gao X G. 2004. Precipitation estimation from remotely sensed imagery using an artificial neural network cloud classification system. Journal of Applied Meteorology, 43 (12): 1834 – 1852 [DOI: 10.1175/JAM2173.1]

Hu B, Du H L and Xiao Y. 2005. Identification of heavy rain with movement of maximum temperature-gradient zone around cloud cluster center. Meteorological Science and Technology, 33(5): 401 – 403

Hu Y N and Li S. 2012. Detection of thunderstorm clouds based on FY2D geostationary satellite // China Conference, S1: Severe Weather Research and Forecasting. Beijing: Chinese Meteorological Society

Jiang J X and Fan M Z. 2002. Convective clouds and mesoscale convective systems over the Tibetan Plateau in Summer. Chinese Journal of Atmospheric Sciences, 26(2): 263 – 270

Li S, Liu J W and Liu Y L. 2010. Detection of strong convective clouds based on FY2D geostationary satellite. Meteorological, Hydrological and Marine Instruments, 27(2): 72 – 78 [DOI: 10.3969/j.issn.1006 – 009X.2010.02.020]

Lin C C, Zhang C A, Lin Z M, Lin X M, Xie Y F and Zheng S Z. 2003. Study on the relationship between brightness temperature from GMS-5 infrared cloud imagery and surface rain rates during the raining seasons of Fujian province. Journal of Tropical Meteorology, 9 (1): 74 – 79 [DOI: 10.3969/j.issn.1006 – 8775.2003.01.009]

Liu Y A, Wei M, Gao W and Li N. 2012. Short-term automatic forecast algorithm of severe convective cloud identification using FY-2 IR images. Journal of Remote Sensing, 16(1): 79 – 92

Lu N M and Wu R Z. 1997. Strong convective cloud characteristics derived from satellite cloud picture. Quarterly Journal of Applied Meteorolgy, 8(3): 269 – 275

Mahrooghy M, Younan N H, Anantharaj V G and Aanstoos J. 2011. High resolution satellite precipitation estimate using cluster ensemble cloud classification // Proceedings of the 2011 IEEE International Geoscience and Remote Sensing Symposium (IGARSS). Vancouver: IEEE: 2645 – 2648 [DOI: 10.1109/IGARSS.2011.6049746]

Mahrooghy M, Younan N H, Anantharaj V G and Aanstoos J. 2012. On the use of a cluster ensemble cloud classification technique in satellite precipitation. IEEE Journal of Selected Topics in Applied Earth Observations and Remote Sensing, 5(5): 1356 – 1363 [DOI: 10.1109/JSTARS.2012.2201449]

Teng W P, Du H L, Hu B and Yu S X. 2006. IR image characteristics of raining cloud clusters and relationship with hourly rainfall in Zhejiang province. Meteorological Science and Technology, 34(5): 527 – 531

Vicente G A, Scofield R A and Menzel W P. 1998. The operational GOES infrared rainfall estimation technique. Bulletin of the American Meteorological Society, 79(9): 1883 – 1898 [DOI: 10.1175/1520 – 0477(1998)079 <1883: TOGIRE>2.0.CO;2]

Yu X D, Zhou X G and Lemon L. 2010. Severe Convective Weather Nowcasting. Beijing: CMA Training Centre, 18 – 29

Zhang J, Wang M and Gu Q Y. 2007. Analysis on corresponding relation of TBB and rainstorm on September 3, 2006 in Sichuan. Journal of Sichuan Meteorology, 27(2): 7 – 9.

Zhao Q and Cheng L. 2009. Analysis and application of brightness temperature on cloud top in a regional rainstorm. Journal of Shaanxi Meteorology, (4): 1 – 4

Zheng S L and Xi S P. 2006. Analysis on severe convection weather on June 21, 2005 in He'nan. Meteorology Journal of He'nan, (3): 46 – 47 [DOI: 10.3969/j.issn.1673 – 7148.2006.03.027]

Zhu P, Li S C and Xiao J S. 2012. Preliminary study on application of radar auto-warning technology to short-time strong convective weather forecasting in Qinghai. Torrential Rain and Disasters, 31(2): 182 – 187

青藏高原东部暴雨云团局地强降水响应特征

朱平[1,2,3]，李生辰[3]，王振会[1,2]，肖建设[4]

1. 南京信息工程大学 气象灾害省部共建教育部重点实验室，江苏 南京 210044;
2. 南京信息工程大学 大气物理学院，江苏 南京 210044;
3. 青海省气象台，青海 西宁 810001;
4. 青海省气象科研所，青海 西宁 810001

摘 要: 为研究青藏高原(简称“高原”)东部暴雨云团的局地强降水响应特征,使用 FY-2 卫星红外通道数据,选择降水开始前 4 小时直到降水结束后 2 小时的时段,对高原东部 19 次典型局地暴雨过程分两种方式进行云团分析,第一种方式为针对测站上空 7×7 像元范围的云团进行云顶温度变化等相关分析,第二种方式为对关键四省范围内的云团进行识别和追踪,并计算对流云团参数。对暴雨云团的雷达回波特征也进行了分析。结果表明:(1) 7×7 像元范围红外各通道的云顶温度变化趋势一致,降水阶段云顶温度先降后升,云顶温度梯度先升后降。云顶温度梯度极大值 G_{max} 的峰值和半小时内 G_{max} 的最大上升变化值 ΔG_{max} 均出现在强降水前(0—11 h),G_{max} 峰值次数为 1—2 次,云顶温度极小值 T_{min} 的谷值多出现在强降水之前,T_{min} 曲线斜率大值阶段对应 G_{max} 的大值阶段,ΔG_{max},G_{max} 和 T_{min} 的极值分别可达到 22.3℃,48.3℃和 −90.3℃。(2) 用 7×7 范围云顶温度及温度梯度建立的降水量级预报方程能较好地模拟小时降水量随时间的变化趋势且有一定的预报提前时间,预报误差在 1 个降水量级内。在考虑了 G_{max} 峰值对强降水的贡献后 R^2 由 0.23 提高到 0.54,模拟的降水量峰值与真值峰值明显接近。(3) 对流云团的识别追踪方法更简单有效,对形变较小的云团(相关系数≥0.5)的准确率为 100%,对发生了合并或分裂等严重形变的云团(一般相关系数<0.5)的识别结果正确而追踪结果无效;(4) 高原东部暴雨云团均为中-β—中-α 尺度,水汽柱深厚但强度比低海拔地区更弱,测站暴雨开始之前多数有对流云团覆盖,若对流云团空间参数位置靠近测站,当空间距离至少小于或等于 15 个像距时降水或强降水将在几小时内产生。(5) 暴雨云团在雷达回波图上表现为强降水超级单体风暴特征,且暴雨测站 7×7 范围 G_{max} 峰值时刻对应有回波顶高度(18 dBz)的梯度极大值,红外 1、红外 2 和红外 3 通道的 T_{min} 谷值时刻分别对应回波顶高度极大值和垂直累积液态水含量的极大值。本研究结果对高原强对流云团的识别、跟踪及短时降水预报等具有重要参考价值。

关键词: 红外通道,局地暴雨云团,识别和跟踪,短时降水预报

中图分类号: P457.6 **文献标志码:** A

引用格式: 朱平,李生辰,王振会,肖建设. 2014. 青藏高原东部暴雨云团局地强降水响应特征. 遥感学报,18(2): 405 −431

Zhu P, Li S C, Wang Z H and Xiao J S. 2014. Characteristics of rainstorm cloud clusters to local heavy precipitation over the eastern Qinghai-Tibet Plateau. Journal of R emote Sensing, 1 8(2): 405 −431 [DOI: 10.11834/jrs.20143069]

1 引 言

2004 年 10 月 19 日以来,中国成功发射了 3 颗气象业务卫星(FY-2C、FY-2D 和 FY-2E),具有红外(IR1 即红外 1,10.3—11.3 μm,IR2 即红外 2,11.5—12.5 μm,IR3 即红外 3(水汽通道):6.2—7.6 μm),短波红外(3.5—4.0 μm)以及可见光(0.55—0.9 μm) 5 个通道,其分辨率各不相同。红外通道是昼夜云和地表反射的红外辐射信息,水汽通道得到的是空间大气中上层水汽分布。从这些不同通道得到的各种云图信息,通过加工处理后,可以得到很多卫星气象图像和气象业务产品。目前运用各通道得到的云图信息进行降水估计的应用较为广泛。Adler 和 Negri (1988) 结合 1 维云模式提出

收稿日期: 2013-04-12; 修订日期: 2013-08-16; 优先数字出版日期: 2013-08-25
基金项目: 青海省科技厅项目(编号: 2011-Z-712);公益性行业(气象)科研项目(编号: GYHY201306006)
第一作者简介: 朱平(1980—),女,博士研究生,主要从事大气遥感与短临天气预报研究。E-mail: ping_xjs2010@126.com

了一种估计对流云和层状云降水的方案; Vicente 等人(1988)发展了全自动的卫星估测降雨技术并进行了业务试运行。Lin 等人(2003)使用1998和1999年雨季GMS-5红外云图资料研究云顶亮温和地表降水率之间的关系,得出“随着亮温降低和亮温梯度增加很可能出现强降水”的结论。Hong 等人(2004)使用人工神经网络云分类系统(PERSIANN CCS)进行卫星估测降水,该云分类系统每隔30 min从10.7 μm静止卫星红外云图提取出局地和区域云特征进行细尺度((0.04°×0.04°)/像素)降水分布估测,其小时降水分布估计值和雨量计测量值的相关系数为0.45。Bergès 等人(2009)使用一种改进的云增长率指数法估测降水,该指数相比冷却指数能更有效地识别出降水单体,将该新指数法用于大范围降水估测,其日降水检验结果有所改善。Mahrooghy 等(2011,2012)将链接聚类集成方法(LCE)应用于高分辨率卫星估测降水算法(HSPE)—人工神经网络云分类法估测降水的修正形式,研究结果表明LCE法相比使用自组映射SOM的高分辨率卫星降水估计能力更高,LCE法对中到大雨的Heidke技能评分提高5%至7%,且同等威胁指数ETS在冬季的检验评分提高5%。卢乃锰和吴蓉璋(1997)研究得出在弱降水区对流云团的降水强度与云团的云顶温度梯度呈正相关。但在强降水区,相应的云顶温度梯度却在减小,即很强的降水更容易发生在云顶比较平坦的区域。江吉喜和范梅珠(2002)将青藏高原对流云的强度按云顶温度值分为4级:Ⅰ.即一般性对流云(-32—-54℃);Ⅱ.伴有雷暴的较强对流云(-54—-64℃);Ⅲ.穿越对流层顶的强对流云(-64—-80℃);Ⅳ.极强对流云(≤-80℃),并研究得出高原上对流云的云顶亮温多为-32—-54℃,强对流云很少。胡波等人(2005)根据云团强中心附近的最大亮温梯度区的移动来估计云团未来1小时强降水可能的强度与落区。郑世林和席世平(2006)研究得出云顶亮温梯度大的区域是灾害性天气的易发区。陈佩燕等人(2006)分析得出西北太平洋热带气旋强度(TC)与云顶亮温TBB存在负相关关系。滕卫平等人(2006)分析得出随着云顶亮温的降低,1小时降水量降水强度逐渐增大,出现强降水的机率也明显增多。张驹等人(2007)研究发现TBB值由最低值快速上升时,其对应站点的降水强度也大,降水区域出现在TBB梯度大的地方。赵强和程路(2009)研究得出强降水区域与TBB低值中心对应较好,单站TBB值与降水强度对应较好,TBB低值出现时段与强降雨时段基本吻合。李森等人(李森 等,2010; 胡渝宁和李森,2012)通过计算深对流指数和红外通道亮温差来识别暴雨云团,并得到卫星深对流指数的大值区和红外多光谱带差值的正负分布与对流云的发展、强对流的发生有很好的对应关系。刘延安等人(2012)基于FY2红外云图的亮温和面积阈值实现对强对流云团的短时预报,并得出雨量站实测的1小时降水量与云顶平均亮温和TBB极小值存在较好的对应关系。

青藏高原东部属于干旱、半干旱地区,随着近年来极端天气事件增多,高原上夏季对流活动明显增强,短时强降水异常频发,常导致山洪灾害等。由于高原地形起伏大、降水分布不均,对流降水受地形影响大。然而,东部目前仅两部雷达用于监测和预警强对流天气,探测范围有限;数值预报模式对局地对流降水无能为力,且高原南部常年被云覆盖,因此,本文利用FY-2卫星红外通道监测资料对东部的局地暴雨过程进行分析,并得出红外通道物理量的变化特征及其与1小时降水量之间的关系等,进而提高短时强降水预报的准确率,从而在一定程度上减轻灾害性天气造成的损失。

2 资料说明

选取2005年—2010年发生在青藏高原东部19次典型局地暴雨过程,如表1所示,降水起止时间用年月日时表示,如个例1的降水起止时间为2005年8月14日18:00至15日6:00时。1小时最大降水量 OHP_{max} 栏表示自动气象站测得 OHP_{max} 的时间。高原东部包括13个自动气象站,站点分布位置如图1所示,每个县仅1个自动气象站,站点间的最短

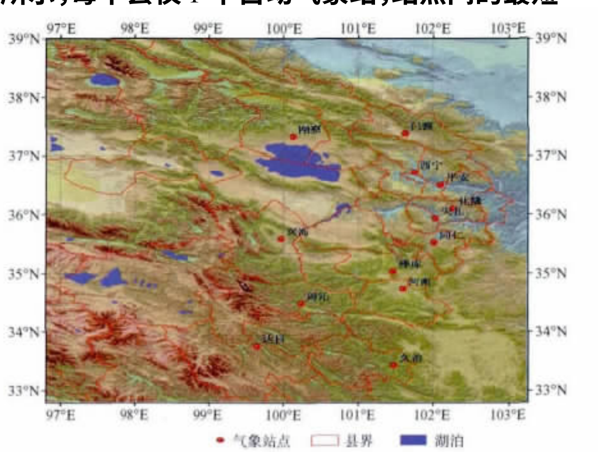

图1 青藏高原东部典型暴雨过程自动测站分布

表 1 青藏高原东部 19 次局地暴雨过程(北京时间)

个例	站号	站名	降水起止时间	OHP_{max}(mm)/时间
1	56043	玛沁	2005-08 1418-1506	27.0/24:00
2	56046	达日	2006-07 1210-1216	25.0/16:00
3	56067	久治	2006-07 2020-2107	27.5/02:00
4	56065	河南	2007-07 1616-1622	25.1/22:00
5	52765	门源	2007-08 0713-0720	28.0/19:00
6	52754	刚察	2007-08 2014-2101	33.0/20:00
7	52866	西宁	2007-08 2514-2606	28.0/22:00
8	52943	兴海	2008-07 2811-2823	25.8/17:00
9	56065	河南	2009-07 1513-1522	32.7/19:00
10	52963	尖扎	2009-08 0214-0308	27.1/01:00
11	52943	兴海	2009-08 2412-2505	27.5/18:00
12	52963	尖扎	2010-05 2819-2902	25.1/01:00
13	52875	平安	2010-08 0711-0718	25.0/17:00
14	52968	泽库	2010-08 1013-1100	27.3/19:00
15	52968	泽库	2006-07 2112-2121	29.1/18:00
16	52765	门源	2006-09 0315-0401	26.1/21:00
17	56065	河南	2009-07 2011-2018	49.1/17:00
18	52877	化隆	2010-08 0711-0719	25.1/17:00
19	52974	同仁	2010-09 2015-2102	36.6/21:00

距离仅 30 km(尖扎到化隆站)。降水实况资料来源于青海省气象台,卫星数据来源于国家卫星气象中心 FY-2C 和 FY-2E 数据(HDF5 格式),提取出包括青海在内的 4 个省范围(72.89°E—108.73°E,25.74°N—50.60°N)的红外云图灰度数据及对应定标表,由此得到该范围的云顶亮温数据。图像分辨率为 0.05°/像素,即约 5 km/像素。

3 固定小范围云顶温度变化特征分析

从图 1 中可看出高原东部的占地面积和地形起伏都比较大,各气象站均分布在山谷里,最短站间距已超过中国山区自动气象站的平均站间距。参考中小尺度强对流云核的直径(约 10—20 km)、全国山洪灾害重点防治区自动气象站的站间距(20—40 km)和山区自动气象站的站间距(平均 <25 km)。假设自动站(图 1)测得降水量能代表周围 15 km 范围的降水,选取以站点为中心的 35 km×3 5 km 矩形云区范围(图 2)作为研究区域,以分析判断测站上空对流云的发展变化和与降水的关系。图 2 为 $M \times N$ 个像素点的矩形范围,取 $M = N = 7$,每个方块表示一个像素点,黑色方块为测站所在位置。

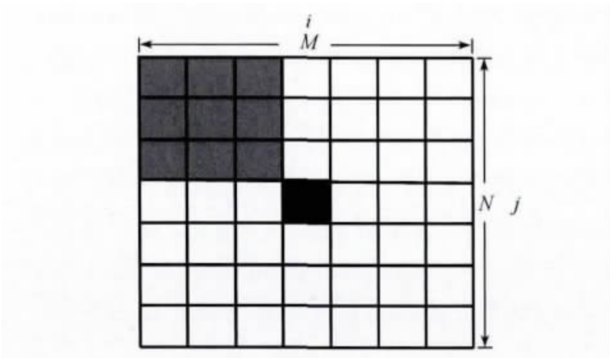

图 2 测站所在计算区域示意图

研究指出(卢乃锰和吴蓉璋,1997;郑世林和席世平,2006;滕卫平 等,2006;张驹 等,2007;赵强和程路,2009),云顶温度梯度和云顶温度极小值均与降水存在较好对应关系。云顶温度降低说明云顶高度升高、积云发展,云顶温度升高表明云顶高度降低、积云减弱;同理,云顶温度梯度也反映了积云的发展变化,云顶温度梯度增大或减小代表云顶局部温度分布(或云顶高度分布)不均一性程度增强或减弱。对表 1 中各次暴雨过程取降水开始前 4 小时直到降水结束后 2 小时的所有时次云图资料,针对研究区域的云块,计算红外通道(IR1、IR2 和 IR3)云顶温度极小值 T_{min} 以及云顶温度梯度的极大值 G_{max}。采用 3×3 窗口(如图 2 灰色区域所示)计

算云顶温度梯度：

$$G = \sqrt{[T(i+1,j) - T(i-1,j)]^2 + [T(i,j+1) - T(i,j-1)]^2} \quad (1)$$

式中，i、j 为象素坐标，T 为云顶温度（单位为℃，T = TBB −273.16）。在图 2 所示 7×7 矩形范围内搜索各个 3×3 窗口中心点的温度梯度，从而得出温度梯度最大值 G_{max}。

3.1　云顶温度极值及提前时间分析

分析表 1 中 19 次降水过程的 7×7 矩形范围云顶温度极值和相对于最大小时降水量整点测量时刻 t_{ohpmax} 的提前时间，由于降水过程 G_{max} 峰值出现 1—2 次，因此列出 IR1 通道的计算值：$t_{\Delta G_{max}}$、$t_{1G_{max}}$、$t_{2G_{max}}$ 和 $t_{T_{min}}$ 分别表示半小时内 G_{max} 最大上升变化值（ΔG_{max}）、G_{max} 第 1 次峰值（G_{1max}）、G_{max} 第 2 次峰值（G_{2max}）、T_{min} 最小谷值相对于 t_{ohpmax} 的提前时间，如表 2 所示（空白处表示未出现 G_{max} 第 2 次峰值），$t_{\Delta G_{max}}$、$t_{1G_{max}}$、$t_{2G_{max}}$ 和 $t_{T_{min}}$ 的范围分别为 2—11 h、1—10.5 h、0—3 h、0—10 h（个例 1—15）或 −0.5— −2.5 h（个例 16—19），ΔG_{max}、G_{1max}、G_{2max} 和 T_{min} 最小谷值分别为 3.4—22.3℃、13.2—48.3℃、16.4—51.2℃和 −40.6— −90.3℃，其中个例 3、14、15、17 降水过程的 T_{min} 谷值均属于 ≤ −80℃的极强对流云顶温度范围（江吉喜和范梅珠，2002）（等级Ⅳ），其余 3 种等级的降水过程各 5 次。19 次局地暴雨过程中有 15 次在小时最强降水结束前出现 G_{max} 第 2 次峰值，$t_{2G_{max}} > 0$ 占 12/15 次，$t_{\Delta G_{max}} > t_{2G_{max}}$ 占 14/15 次，$t_{\Delta G_{max}} > t_{1G_{max}}$ 占 10/19 次。4 次过程在小时最强降水结束前仅出现 1 次 G_{max} 峰值，$\Delta G_{max} < 8$ 的共 3 次，其中 1 次 $G_{1max} >$ 30℃，另外两次 $G_{1max} >$ 13℃，但 T_{min} 分别为 −43℃和 −82.3℃且 $t_{T_{min}} > 1$ h；$\Delta G_{max} >$ 8℃的 1 次 $G_{1max} >$ 40℃。19 次暴雨过程中有 18 次降水与云顶温度具有一定相关关系（个例 10 除外）：当 $G_{2max} >$ 15℃时，强降水将在 3 小时内产生；当 $\Delta G_{max} >$ 8℃且 $G_{1max} >$ 15℃，或 $G_{1max} >$ 30℃，或 $T_{min} <$ −60℃，满足其中之一则强降水在未来 6 小时内产生。

19 次降水过程的 G_{max} 峰值均出现在小时最强降水结束之前；个例 1—15 的 T_{min} 谷值也出现在最强降水结束之前；个例 16—19 的 T_{min} 谷值则出现在小时最强降水结束之后。个例 1—19 说明测站最强降水可能出现在 7×7 范围积云发展到最大高度之后也可能出现在最大高度之前，但一定出现在 7×7 范围积云云顶出现最大温度梯度（即出现最大高度梯度）之后，强降水的具体产生时间及雨强大小视降水所需的热力、动力和水汽条件的具体配置情况而定。

表 2　青藏高原东部 19 次局地暴雨过程 7×7 范围云顶温度极值和提前时间

个例	$t_{\Delta G_{max}}$/h	ΔG_{max}/(℃/0.5 h)	$t_{1G_{max}}$/h	G_{1max}/℃	$t_{2G_{max}}$/h	G_{2max}/℃	$t_{T_{min}}$/h	T_{min}/℃	T_{min} 等级
1	7.0	12.7	5.5	27.4	3.0	16.4	5.0	−53.3	Ⅰ
2	2.5	13.1	1.0	46.1	—	—	1.0	−49.8	Ⅰ
3	2.5	3.4	2.5	16.4	—	—	1.5	−82.3	Ⅳ
4	5.5	15.4	5.0	31.2	0.5	19.5	3.5	−74.3	Ⅲ
5	5.0	8.2	3.5	25.1	0	20.1	0.5	−50.7	Ⅰ
6	2.0	19.3	2.0	28.0	1.0	33.3	0.5	−40.6	Ⅰ
7	2.0	8.2	4.0	20.1	2.0	24.8	0	−59.7	Ⅱ
8	4.0	13.5	4.0	29.1	1.5	29.2	1.5	−62.9	Ⅱ
9	4.0	14.1	3.5	28.9	1.5	33.7	1.5	−69.0	Ⅲ
10	11.0	4.1	10.5	13.2	—	—	10.0	−43.0	Ⅰ
11	3.0	22.3	3.0	37.4	1.0	44.7	1.0	−62.6	Ⅱ
12	2.5	8.2	3.5	16.4	1.5	27.0	4.0	−60.5	Ⅱ
13	2.5	19.4	2.5	35.6	1.0	44.3	0.0	−69.5	Ⅲ
14	4.0	13.6	4.0	42.2	2.5	43.2	1.5	−84.6	Ⅳ
15	3.0	10.8	2.5	38.5	1.0	30.1	0.5	−90.3	Ⅳ
16	2.0	9.0	2.0	22.8	0	30.2	−2.0	−69.8	Ⅲ
17	2.0	15.4	1.5	33.7	0	39.6	−2.5	−85.4	Ⅳ
18	2.5	19.8	2.0	48.3	1.0	51.2	−2.0	−69.1	Ⅲ
19	3.0	6.4	1.0	32.2	—	—	−0.5	−60.3	Ⅱ

3.2 云顶温度变化趋势分析

以2005年8月14日玛沁暴雨过程(个例1)和2010年9月20日同仁暴雨过程(个例19)为例,分别说明T_{min}谷值出现在小时最强降水结束前和结束后的云顶温度变化趋势特征。从图3和图4可以看出,整个降水过程红外通道(IR1、IR2和IR3)的T_{min}变化趋势基本一致,G_{max}的变化趋势也基本一致,特别是IR1和IR2通道的云顶温度值接近;降水开始前4小时直到降水结束2小时内,IR1和IR2通道的云顶温度值可为正值,但IR3(水汽)通道的云顶温度始终小于-20 ℃,表明暴雨过程的水汽柱深厚,达到了对流层中上层。降水开始前(图3和图4中左侧负值的绿色柱形),云顶温度逐渐降低、积云发展、云高升高,图3在16:00—16:30出现了积云的短时减弱,对应云顶温度稍有升高、云顶温度梯度略有减小;图4在降水开始前的积云基本处于不断发展中。降水阶段(图3和图4中1小时降水量大于或等于0的绿色柱形,测得降水的第一个整点分别为18:00和15:00),积云继续发展成熟,由于降水释放的潜热增加了大气环境温度,图3和图4分别在降水开始的1小时内出现了云顶温度升高。随着降水进行,云顶高度先升后降,积云逐渐减弱,降水结束后云顶温度恢复到环境大气的平衡状态。图3中T_{min}从谷值升高的过程中,出现较明显的两次降低,表明积云在从最大高度降低的过程中会出现短时增长现象。从图3和图4中还看出,G_{max}曲线大值阶段对应T_{min}曲线斜率大值阶段,如图3中17:00—1 9:30,19:30—00:30和图4中17:30—23:00的T_{min}曲线陡度与G_{max}曲线值。

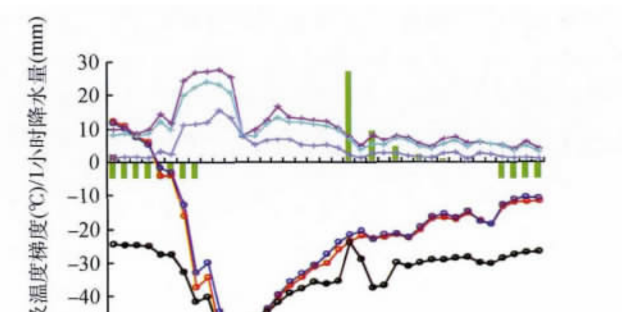

图3 2005年8月14日玛沁暴雨过程云顶温度变化图

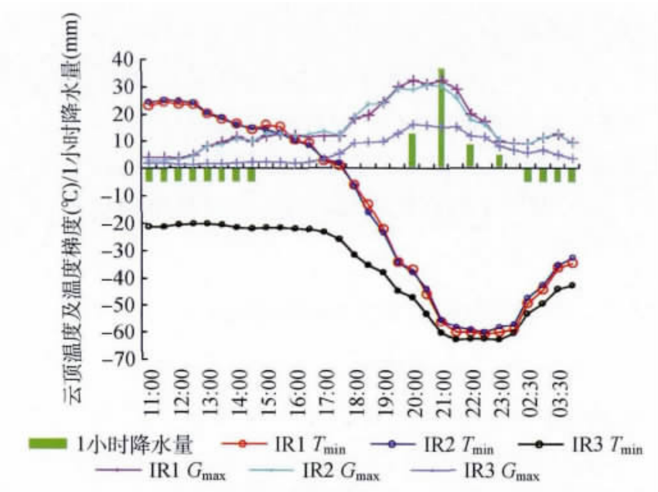

图4 2010年9月20日同仁暴雨过程云顶温度变化图

根据19次局地暴雨过程的具体降水时间,选择恰当的降水时段以分析降水过程的云顶温度变化总趋势。图5中以横轴$t-$表示降水开始前3小时,t表示小时最强降水结束时刻,$t-1$、$t-2$、$t-3$表示t前3小时,$t+1$、$t+2$、$t+3$表示t后3小时,$t--$表示降水结束后2小时。从图5中可以看出,红外各通道的云顶温度及温度梯度变化趋势分别一致,IR1和IR2通道的计算值很接近,IR3(水汽)通道的云顶温度在-20 ℃以下,G_{max}峰值出现在降水开始直到t时刻这一阶段;降水阶段云顶温度先降低后上升、云顶温度梯度先上升后下降、对应积云高度先增长后减小,降水结束后2小时云顶温度逐渐恢复平衡。前15次局地暴雨过程,降水开始前3小时云顶温度略有先降低后上升趋势,如IR1通道云顶温度依次为-67.17℃、-66.63℃、-68.41℃;$t-1$时刻云顶温度为最低、对应云顶温度梯度最大。后4次局地暴雨过程,降水开始前3小时云顶温度逐渐下降,t时刻云顶温度梯度为最大值,$t+2$时刻云顶温度为最低、对应积云高度达到最大高度。

3.3 小时降水量级预报方程及误差检验

根据上述分析,选择IR1和IR3通道的云顶温度极小值(x_1和x_2)、IR1通道的云顶温度梯度极大值(x_3)等作为自变量,小时降水量作为因变量(y)。根据青海省短时降水强度的划分标准(朱平 等,2012):0 mm≤y<8 mm为普通降水(Ⅲ级),8 mm≤y<16 mm为短时强降水(Ⅱ级),y≥16 mm为短时暴雨(Ⅰ级)。选择小时降水量大于1 mm的62个降水时次,建立多元回归方程:

$$y = 0.61 + 0.01x_1 - 0.11x_2 + 0.45x_3 \quad (2)$$

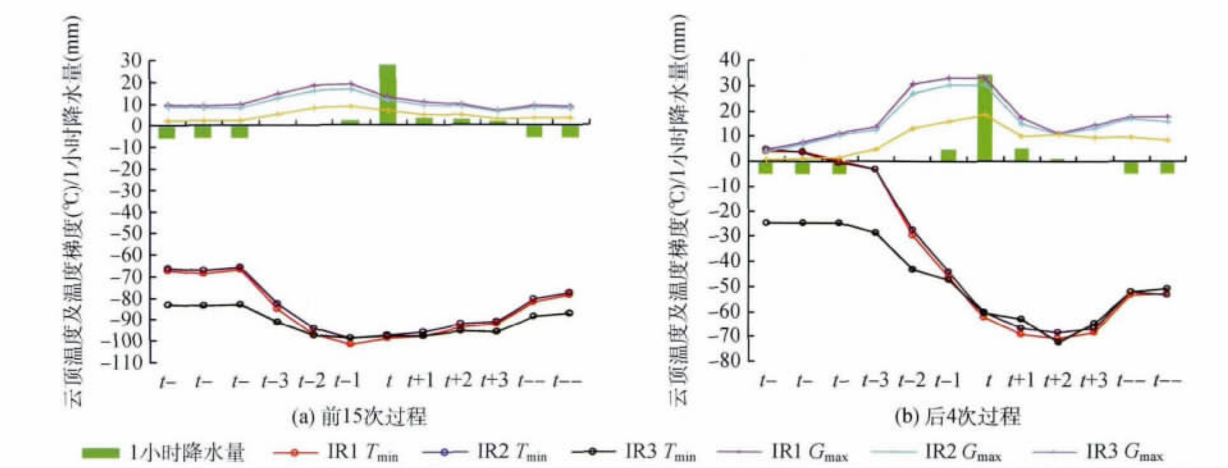

图 5 青藏高原东部 19 次局地暴雨过程云顶温度变化总趋势图

该方程通过 $P<0.01$ 的检验,R^2 为 0.23(仅能解释因变量 23% 的变异)。由于 x_3 的峰值均出现在小时最强降水结束之前,因此认为 x_3 峰值对小时最大降水量起重要贡献,x_3 峰值对 y 的贡献为:

$$y = -2.58 + 1.03x_3 - 0.01x_3^2 \quad (3)$$

该方程通过 $P<0.01$ 的检验(相关性可信度至少为 99%),R^2 为 0.55。加入 x_3 峰值的贡献后所得多元回归方程为:

$$y = -2.09 + 0.12x_1 - 0.16x_2 + 0.65x_3 \quad (4)$$

该方程通过 $P<0.01$ 的检验,R^2 提高到 0.54,能较好地模拟小时降水量随云顶温度变化的趋势。

假设 t 仍为小时最强降水结束时刻,根据 1 小时降水量的真值分布时间,选择降水时段为 $t-1$—$t+3$,对式(2)—(4)进行小时降水量预报检验,对于自变量 x_1—x_3 的真值分为 t 时刻不使用 x_3 峰值和使用 x_3 峰值贡献两种情况。检验结果如图 6 所示,$R^2=0.23$、$R^2=0.55$ 和 $R^2=0.54$ 分别代表使用式(2)、式(3)和式(4),可见方程模拟结果基本能反映真值随时间的变化趋势,模拟计算的峰值与真值的峰值差别均在 1 个量级内。前一种情况的模拟结果能提前 1 小时预测到强降水,但模拟计算值与真值相差 1 个量级;后一种情况模拟计算的峰值与真值明显接近,但提前时间在 0.5 h 内。总的来看,考虑 x_3 峰值对强降水影响的 $R^2=0.55$ 和 $R^2=0.54$ 的模拟计算值与真值更为接近,可见云顶最大温度梯度及梯度峰值对小时降水量起到了重要贡献。

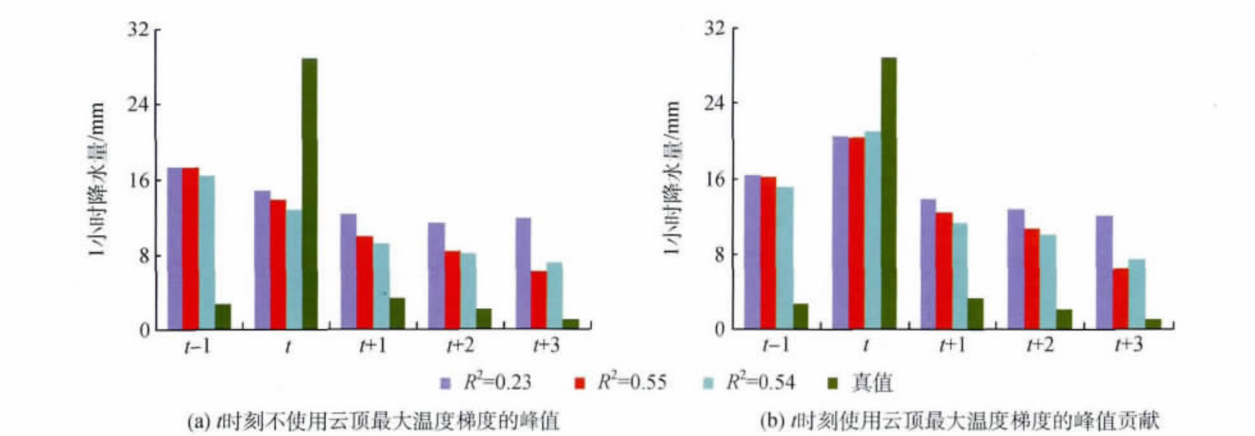

图 6 局地暴雨过程小时降水量级预报检验结果对比图

另外,对 19 次局地暴雨过程降水开始前 3 小时内红外通道云顶温度极小值和温度梯度最大值进行统计分析。IR1 通道的云顶温度极小值(x_1)和云顶温度梯度极大值(x_3)分别为 8.6— −74.7℃和 4.1—40.6℃,IR3 通道的云顶温度极小值(x_2)为 −21.8— −68.7℃。该 19 次过程中仅两次过程(个例 5 和个例 6)在降水开始前 3 小时内的 IR1 云顶温度极小值大于 0℃。因此,可将同时满足 $x_1<0$℃,$x_2<-20$℃ 和 $x_3>4$℃ 作为即将有降水产生的先兆条件。

4 对流云团与测站降水

4.1 对流云团的识别和跟踪

对相邻时次的云图,选择云顶温度阈值(江吉喜和范梅珠,2002)并提取轮廓,若轮廓内像元个数大于或等于100个,则认为是对流云团;计算云团质心间相距100 km以内的云团相关系数,以同时满足最短质心距离和最大相关系数的云团为最佳匹配云团。

步骤1 取 T_C 为 −32℃以提取云团轮廓,计算轮廓内像元个数 n_c,若 $n_c \geqslant 100$,则认为是一般性对流云团(江吉喜和范梅珠,2002);继续寻找对流云团内的最低温度 $T_{\min}$,若 $T_{\min} \leqslant -80$℃,则取 T_C 为 −54℃以提取轮廓,若该轮廓内 $n_c \geqslant 100$(刘延安 等,2012),则认为是强对流云团(江吉喜和范梅珠,2002);计算云团面积并记录云团代号。表1中19次局地暴雨过程的云团均属于中−β—中−α尺度对流云,面积为2600—1100000 km^2,其中2008年7月28日兴海测站暴雨过程(个例8)个别时次对流云团达到中-α尺度。2006年7月12日(个例2),取 T_C 为 −32℃,14:30—16:00四省范围内对流云团个数分别为18个、18个、14个和18个,该时段达日测站上空云团属于一般性对流云团(云团边界依次对应图7中蓝色、紫色、绿色、玫瑰色轮廓,红色线表示青海省界),云团面积为中−β尺度且面积逐渐增大,从3986.6 km^{2}增加到77059.1 km^2,$T_{\min}$ 从 −48.2℃降低到 −66.4℃,测站15:00—16:00出现强降水。

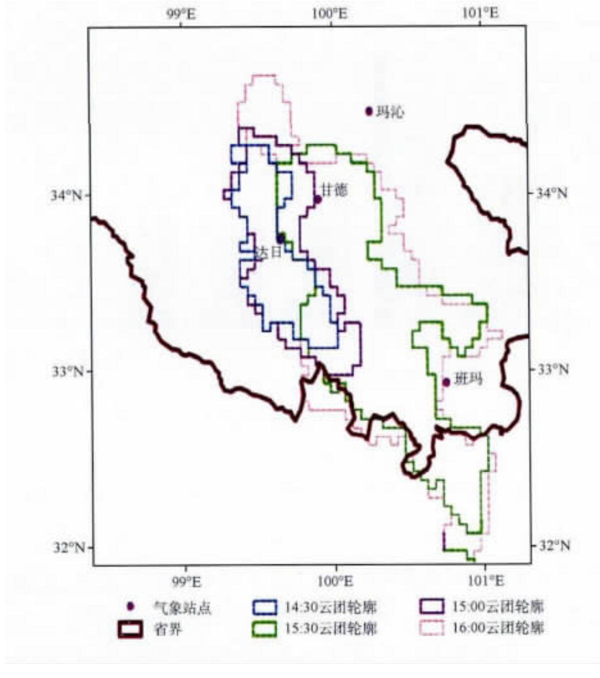

图7 2006-07-12 达日局地暴雨过程 14:30—16:00 对流云团轮廓

步骤2 计算相邻时次云团质心位置(X_{CG},Y_{CG})和相关系数 r:

$$X_{CG}=\frac{\sum_{i=1}^{N_P}X_iT_i}{\sum_{i=1}^{N_P}T_i}\qquad Y_{CG}=\frac{\sum_{i=1}^{N_P}Y_iT_i}{\sum_{i=1}^{N_P}T_i}\tag{5}$$

式中,T_i 为像元温度,为方便提取质心,当 $T_i > -32$℃时,令 $T_i=0$;N_P 为对流云团内所有像元个数;X_i、Y_i 分别为像元经度和纬度。

$$r=\frac{\sum_{j=1}^{m}\sum_{i=1}^{n}\left(T_f(i,j)-\overline{T}_f\right)\left(T_g(i,j)-\overline{T}_g\right)}{\sqrt{\sum_{j=1}^{m}\sum_{i=1}^{n}\left(T_f(i,j)-\overline{T}_f\right)^2}\sqrt{\sum_{j=1}^{m}\sum_{i=1}^{n}\left(T_g(i,j)-\overline{T}_g\right)^2}}\tag{6}$$

式中,$\overline{T}_f$ 和 $\overline{T}_g$ 分别为 f 云团和假想匹配云团 g 的平均云顶温度。以云团质心为中心,m、n 分别为覆盖云团的矩形在经度方向和纬度方向的像元个数。

统计相邻时次最佳匹配对流云团的移动距离(以质心位置为标准)和相关系数,分别为小于100 km和大于0.5。例如,2006年7月12日四省范围的对流云团追踪,14:00时刻0号云团与14:30时刻0—18号云团的相关系数及质心间的距离如表3所示,可见14:00的0号云团恰好与14:30的0号为最佳匹配云团,相关系数为0.9,质心间的距离为21.2 km。

表3 2006-07-12 达日局地暴雨过程 14:30 云团的计算值

云团代号	相关系数	质心距离/km
0	0.9	21.2
1	0.6	1573.0
2	0.7	1181.4
3	0.7	1039.5
4	0.6	1041.1
5	0.5	1025.1
6	0.7	1909.7
7	−0.4	2483.1
8	0.6	2213.4
9	0.6	2406.4
10	0.3	2203.2
11	0.6	2560.1
12	0.6	2966.1
13	0.6	2621.9
14	0.6	2615.7
15	0.6	2665.0
16	0.6	2729.3
17	0.6	2742.6
18	0.0	2970.6

步骤3 令 t_0 时刻0号云团的质心为 $CG_0^{t_0}$,在 t_1 时刻云图上搜索各云团质心 $CG_k^{t_1}$,寻找 $CG_k^{t_1}$ 与 $CG_0^{t_0}$ 相距$\triangle L<100$ km 的云团,计算相关系数 r 时,m、n 的取值以 $CG_0^{t_0}$ 和 $CG_k^{t_1}$ 所在云团的相对较小覆盖范围为准;以同时满足最大相关系数和$\triangle L<100$ km 的最小距离所在云团为 t_0 时刻0号云团的最佳匹配云团。同理可在 t_1 时刻云图上得到 t_0 时刻1、2、3,…,18号云团的最佳匹配云团。此对流云团识别和跟踪方法较简单,计算量相对较小,准确率高。

4.2 云团识别和跟踪效果检验

2010年8月10日泽库测站暴雨过程的对流云团的识别和追踪效果,如图8和表4所示,图8中标有质心点的云团为识别和追踪到的一致的对流云团,13:00—16:00识别和追踪到的对流云团一致;16:30的追踪结果为无,识别到泽库测站附近存在22号对流云团(图8(h)彩色云团)。从13:00的6号云团(图8(a)彩色云团)开始,该云团与13:30的6号云团恰好是最佳匹配云团,最大相关系数为0.7,质心间的距离为36.2 km。13:00—16:00属于一般性对流云团,T_{min}为220.7—196.2 K,即−52.3℃—−76.8℃;从13:00开始泽库西南方向有对流云发展,直到15:30已发展成中−β尺度、T_{min}为198 K的15号云团(表4、图8(f)虚线轮廓内云团),该云团与16:00的17号云团(表4、图8(g)虚线轮廓内云团)是最佳匹配云团,相关系数为0.9,质心距离为21.8 km。从15:30和16:00的云图(图8(f)、(g))可以看出彩色云团与轮廓线内云团有逐渐合并的趋势,直到16:30已合并为22号云团,T_{min}为190 K,属于强对流云团(彩色云团的阈值为−54℃,轮廓线内云团阈值为−32℃),对流云团已发生了严重形变,16:00的15号云团(彩色)和17号云团(轮廓线内)与16:30的22号云团的相关系数分别低于0.5。

其他强降水过程的云团检验结果与之类似,对流云团的识别和跟踪方法对形变较小的云团(相关系数≥0.5)的检验结果准确率为100%,对发生了合并或分裂等严重形变的云团(相关系数<0.5)的识别结果正确而追踪结果无效。

表4 2010年8月10日泽库测站暴雨过程的对流云团识别和追踪计算值

时次	识别的云团代号	T_{min}/K	追踪的云团代号	相关系数	质心距离/km
13:30	6	222.3	6	0.7	36.2
14:00	8	222.9	8	0.7	29.0
14:30	9	209.1	9	0.6	37.6
15:00	11	205.9	11	0.5	74.1
15:30	12,**15**	203.5,**198**	12	0.9,**0.4**	31.7,**243.1**
16:00	15,**17**	198.9,**196.2**	15	0.9,**0.9**	18.5,**21.8**
16:30	22	190	无	0.3,**0.4**	

4.3 对流云团参数计算

根据研究结果,卫星深对流指数的大值区和红外多光谱带差值的正负分布与对流云的发展、强对流的发生有很好的对应关系(李森 等,2010;胡渝宁和李森,2012);雨量站实测的1小时降水量与云顶平均温度和温度极小值存在较好的对应关系(刘延安 等,2012);云顶温度梯度大值区和强降水区的位置对应也较好(胡波 等,2005;郑世林和席世平,2006)。由于高原测站稀疏,本文仅对19次局地暴雨过程的测站上空有对流云覆盖的时次进行分析,选择测站降水开始前3小时和强降水开始前3小时,计算并分析上述强对流云参数(辐射参数和空间参数)与测站降水预报的关系。

(1)辐射参数。对流云团云顶平均温度 $\bar{T}$、最低温度 T_{min}、最大温度梯度 G_{max},质心位置红外多光谱带差值(T_{12}、T_{13})和深对流指数 DCI_{NS}。温度梯度和质心位置的计算式分别同式(1)和式(5)。

$$\begin{cases} T_{12} = T_{CG1} - T_{CG2} \\ T_{13} = T_{CG1} - T_{CG3} \end{cases} \tag{7}$$

式中,T_{CG1}、T_{CG2}和 T_{CG3} 分别表示质心的IR1,IR2和IR3的云顶温度,质心的深对流指数 DCI_{NS}计算式为

$$DCI_{NS} = \begin{cases} 250 - T_{CG} & T_{CG} < 250\ \text{K} \\ 0 & T_{CG} \geq 250\ \text{K} \end{cases} \tag{8}$$

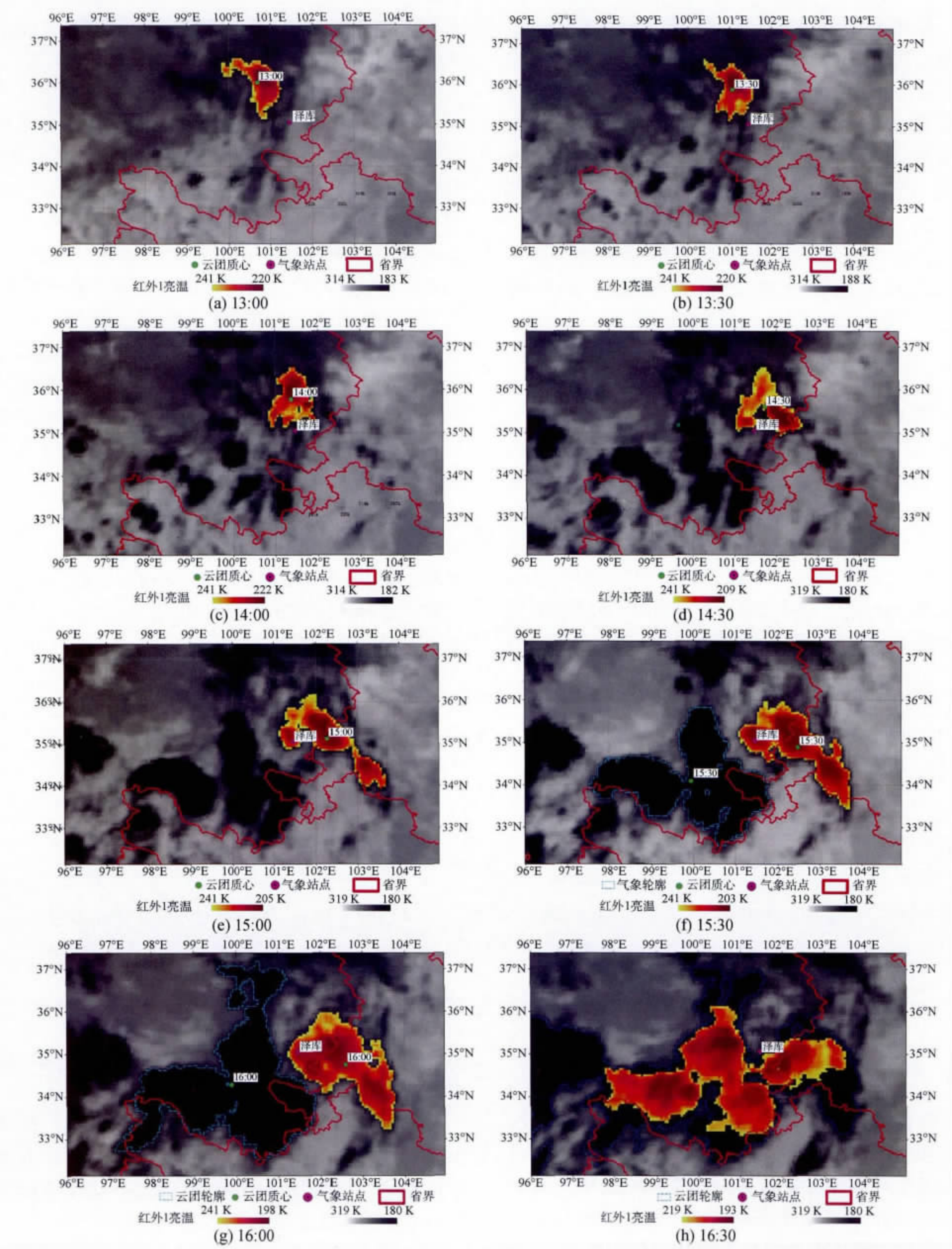

图 8 2010 年 8 月 10 日泽库测站暴雨过程的对流云团追踪效果

式中,T_{CG}为质心位置云顶温度,由于 400 hPa 附近大气的温度一般为 250 K,DCI_{NS}值可以表示云顶等于或高于 400 hPa 深对流云的程度,强对流开始前DCI_{NS}值越大表示发展成强对流云的机率越大。

(2)空间参数。对流云团质心位置(X_{CG},Y_{CG})、最低温度T_{min}位置、最大温度梯度G_{max}位置和测站位置的距离Δl(单位:像元个数),分别为Δl_{CG}、$\Delta l_{T_{min}}$和$\Delta l_{G_{max}}$。

4.4 数据分析和检验

以 -32℃或 -54℃作为对流云团的阈值，19 次局地暴雨过程中除 2009 年 8 月 2 日尖扎测站（个例 10）外，其余 18 次过程在强降水开始前 3 小时内均有对流云团覆盖测站，仅有 3 次过程在开始降水前 3 小时内有对流云团覆盖测站，可见高原夏季云顶温度高于 -32℃也能产生降水，而产生强降水的对流云顶温度一般低于 -32℃。测站强降水开始前 3 小时内对流云团参数值，仅 2010 年 8 月 10 日泽库测站这 1 次暴雨过程的 $T_{12} < -8$℃、$T_{13} < -10$℃以及 $DCI_{NS} \geq 50$，满足低海拔地区强对流雷暴云团的条件（李森 等，2010；胡渝宁和李森，2012），其余过程高原雷暴云团的 T_{12}、T_{13}以及 DCI_{NS}均不满足此条件。强降水开始前 3 小时内有对流云团覆盖测站的过程，最小 $\Delta l \leq 15$ 个像距的过程共 13 次，$\Delta l_{T_{min}}$ 均大于 5，列举出最小 $\Delta l \leq 5$ 的过程的对流云团参数和对应小时最大降水量 OHP，如表 5 所示，t_g 表示最小 Δl 时刻相对于暴雨测站 7×7 范围的云顶最大温度梯度峰值时刻的提前时间，t_{ohp} 表示最小 Δl 时刻相对于暴雨测站最大小时降水结束时刻的提前时间。可见 Δl_{CG} 平均小于 $\Delta l_{G_{max}}$、$\bar{T} \leq -40$℃、$G_{max} \geq 11$℃、$T_{12} \leq -2$、$T_{13} \leq 7$ 以及 $DCI_{NS} \geq 13$。其余降水开始前 $\Delta l \leq 15$ 个像距的局地暴雨过程的结果与之类似。因此若对流云团质心位置或最大温度梯度位置靠近测站（最小 $\Delta l \leq 5$），则 3 小时内一定有降水产生，多数情况下有强降水产生。最小 Δl 时刻可能比测站 7×7 范围的云顶最大温度梯度峰值时刻提前或推后 0—3 h，但均比最大小时降水结束时刻的提前 0.5—3 h。

2005 年 8 月 14 日玛沁测站暴雨过程（OHP 为 27 mm），22:00 时刻 $\Delta l_{G_{max}}$ 为 2 个像元距离，对应 G_{max}为 11℃（表 5）；以玛沁测站为中心的 7×7 范围内（图 9），22:00 时刻的 G_{max} 为 13℃。2009 年 7 月 20 日河南测站的小时最大降水量为 49.1 mm，15:30 时刻 $\Delta l_{G_{max}}$ 为 3 个像距，对应 G_{max} 为 36℃（表 5）；以河南测站为中心的 7×7 范围内（图 10），15:30 时刻的 G_{max} 为 34℃。2006 年 7 月 12 日达日测站的小时最大降水量为 25 mm（表 5），14:30 和 15:00 时刻 Δl_{CG}均为 2 个像距，对应 $\bar{T}$ 为 -41℃和 -44℃，T_{min} 为 -48℃ 和 -56℃；以达日测站为中心的 7×7 范围内（图 11），14:30 和 15:00 时刻 T_{min} 为 -48℃和 -50℃。可见以测站为中心的固定小范围和对流云团的识别追踪两种方式计算的结果均是正确的。

表 5 测站强降水开始前 3 小时内最小 $\Delta l \leq 5$ 过程的对流云团参数

OHP/mm	Δl_{CG}/个像距	$\Delta l_{G_{max}}$/个像距	$\bar{T}$/℃	G_{max}/℃	T_{12}/K	T_{13}/K	DCI_{NS}/K	t_g/h	t_{ohp}/h
25.0	2	13	−41	36	−2	7	23	0.5	1.5
25.1	5	23	−44	29	−7	−7	33	1.5	3.0
27.0	6	2	−40	11	−2	2	13	−1.5	2.0
28.0	3	>35	−41	18	−3	0	26	−2.5	1.0
32.7	4	13	−49	39	−2	−9	34	1.0	2.5
49.1	7	3	−52	36	−2	−4	32	1.5	1.5

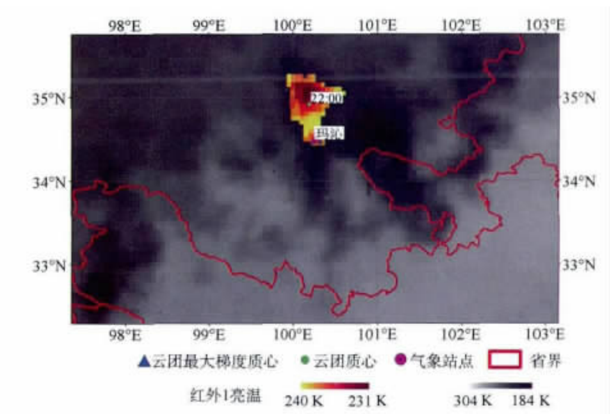

图 9 2005 年 8 月 14 日 22:00 玛沁测站暴雨云团

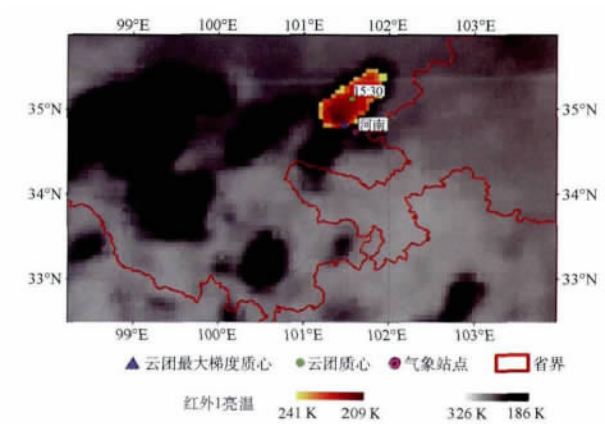

图 10 2009 年 7 月 20 日 15:30 河南测站暴雨云团

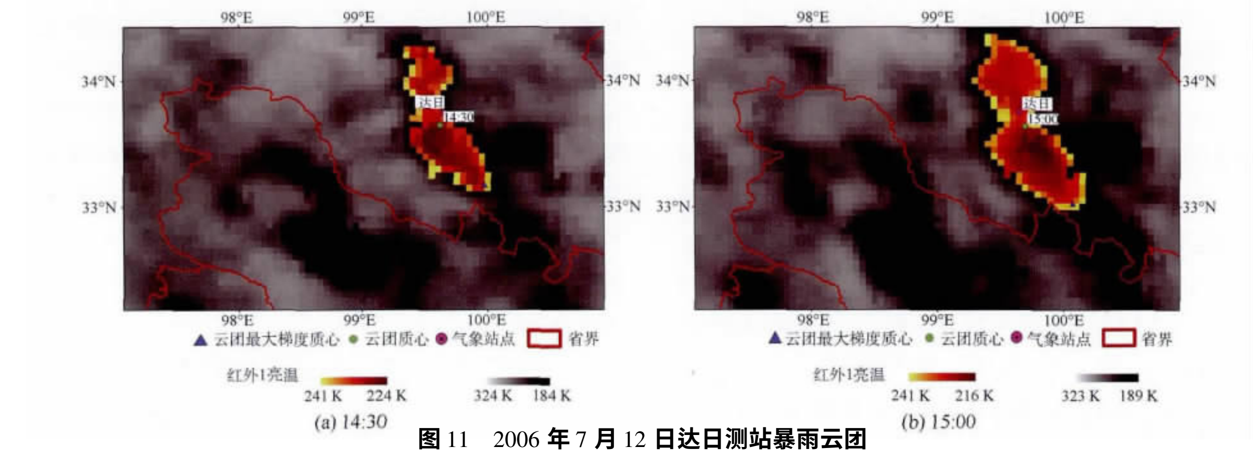

图 11　2006 年 7 月 12 日达日测站暴雨云团

5　暴雨云团局地降水雷达回波特征

2010 年 8 月 7 日平安局地暴雨过程,14:30 从黄南州东移北上的云团与 15:00 从海北州南下的云团合并加强,造成平安在开始降水 1 小时(16:00—17:00)内就产生了暴雨,强降水集中在后半小时并伴有冰雹、雷电和大风天气。以平安为中心的 7 × 7 范围的云顶温度变化(30 min 间隔)如图 12 所示,17 时 IR1 和 IR3 最低云顶温度谷值分别为 –69.5℃和 –60.5℃,16:00 为红外通道云顶温度梯度最大峰值时刻。16:00 7 号暴雨云团(图 13,平安北部)云顶最低温度、低温质心和最大温度梯度位置(云团空间参数位置)与平安测站距离分别为 39、14 和 12 个像距,18 号暴雨云团(图 13,平安南部)最低云顶温度(IR1 为 –64.2℃)位置与平安测站相距 6 个像距,此时恰为平安 7 × 7 范围云顶温度梯度最大峰值时刻。1 6:30 平安北部 7 号云团与南部 18 号云团已经合并,云团空间参数位置与平安测站距离均大于 30 个像距,合并后的云团向东南方向移动。

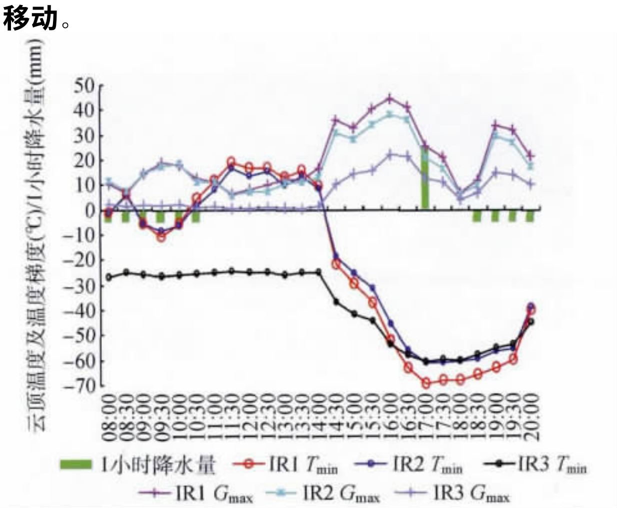

图 12　2010 年 8 月 7 日平安暴雨过程云顶温度变化图

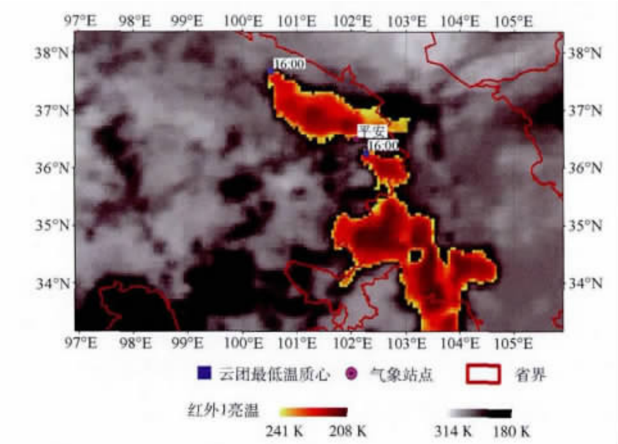

图 13　2010 年 8 月 7 日平安暴雨过程 16 时暴雨云团

2010 年 8 月 7 日红外暴雨云团平安局地强降水过程,中气旋(俞小鼎 等,2010)特征不明显。从雷达回波图(图 14)看出,16:08 平安测站回波顶高海拔 11 km,以平安为中心的 7 × 7 范围的回波最大海拔高度为 15.5 km 且该范围回波顶高度梯度大(图14(a))与 16 时以平安为中心的 7 × 7 范围红外通道云顶温度梯度为最大峰值(图 12)的结果相符。由于 16:30 平安北部 7 号云团与南部 18 号云团已经合并,使处在云团合并区域的平安对流加强,16:32 对流强中心前沿到达平安,最大回波强度(66 dBz)位于平安北部,强中心带及边缘上产生两个对流单体,低层基本反射率因子强回波中心形如弓型(图 14(b)),沿粉色虚线作垂直剖面,可以看到低层径向速度为负的入流到高层径向速度为正的出流(图 14(c)中黄色箭头)、以及低层基本反射率因子梯度和入流一侧(图 14(b)中橙色箭头所示)对应的弱回波区(图 14(d)),最强中心高度低于 3 km,45 dBz 回波顶高(>6 km)高于 18 dBz 回波顶高的一半,因此属于强降水超级单体(俞小鼎 等,2010),该对流风暴向东南方向移动,16:41 平安境内出现较明显的下沉辐散气流(图 14(e)(f)红色椭

圆内),强回波带上有两个对流单体、最大预期冰雹直径为 5 cm 的对流单体位于平安测站,低层基本反射率因子强回波中心形如“S”型(图 14(f)),因入流仍然只有一个,因此仍属于强降水超级单体。16:48 平安的最大垂直累积液态水含量达到 62 kg/m^2(图 14(g)),对流单体最大回波强度为 65 dBz,最强中心高度为 3.9 km,30 dBz 对流顶高大于 12 km。风暴单体继续东南移动,16:55 平安南部最大预期冰雹直径增加到 6 cm(图 14(h)),以平安测站为中心的 7 ×7 范围的回波顶高达到此次过程最大海拔高度 17.1 km(图 14(i)),与 17 时平安 7 ×7 范围的红外通道云顶最低温度谷值的结果一致。

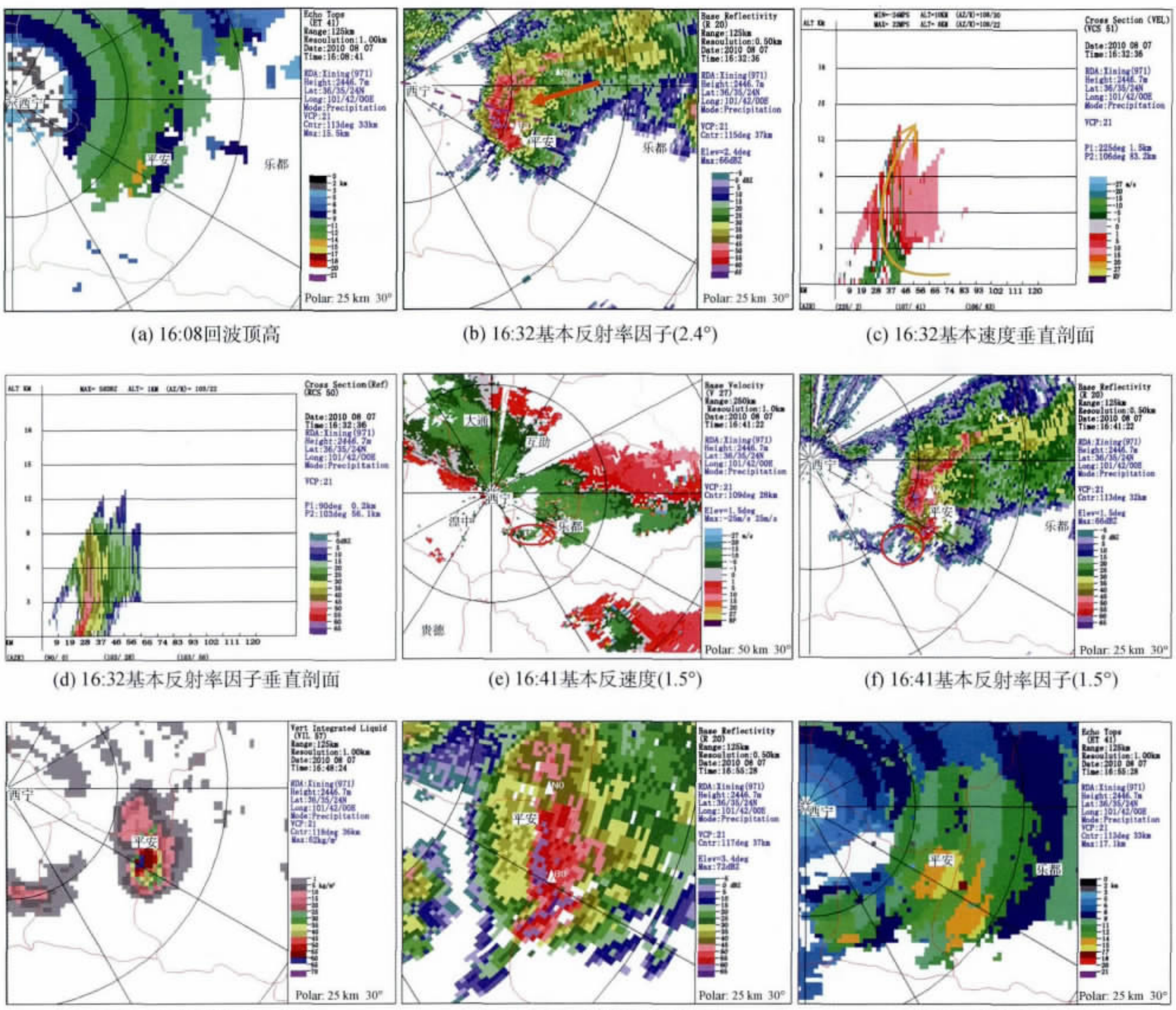

(a) 16:08回波顶高　(b) 16:32基本反射率因子(2.4°)　(c) 16:32基本速度垂直剖面

(d) 16:32基本反射率因子垂直剖面　(e) 16:41基本反速度(1.5°)　(f) 16:41基本反射率因子(1.5°)

(g) 16:48垂直累积液态水含量　(h) 16:55基本反射率因子(1.5°)　(i) 16:55回波顶高

图 14　2010 年 8 月 7 日暴雨云团平安局地强降水雷达回波图

其余局地暴雨过程的雷达回波特征与此类似,暴雨测站 7 ×7 范围的云顶温度梯度最大峰值时刻对应雷达 18 dBz 回波顶高度梯度极大值、IR1 和 IR2 云顶最低温度谷值时刻对应雷达回波顶高度极大值和 IR3 云顶最低温度谷值时刻对应垂直累积液态水含量的极大值。高原东部暴雨云团产生局地强降水过程,在雷达回波图上表现为强降水超级单体对流风暴特征,存在较明显低层高反射率因子梯度和前侧入流对应的弱回波区、以及暴雨阶段的后侧下沉气流,最大回波强度可达到 60 dBz 以上,最大垂直累积液态水含量可达到 50 kg/m^2 以上,最强回波顶高偏下一般低于 3 km,风暴顶高可达到距地 15 km 左右,30 dBz 或 45 dBz 回波顶高大于 18 dBz 回波顶高的二分之一,产生雷雨、冰雹和大风天气。

6　结　论

采用 FY-2 系列的 C 星和 E 星红外通道数据,

选择降水开始前4小时至降水结束后2小时的时段,对青藏高原东部的19次局地暴雨过程分两种方式进行了分析,第1种方式针对测站上空7×7像元范围的云团进行云顶温度变化等相关分析,第2种方式为对关键四省范围内的云团进行识别和追踪,并计算对流云团参数,初步得出了降水或强降水产生的先兆条件和提前时间。并且对暴雨云团的雷达回波特征也进行了附加分析。主要结果如下:

(1)红外通道(IR1、IR2和IR3)的云顶温度及温度梯度变化趋势分别一致,IR1和IR2通道的计算值很接近,IR3(水汽)通道的云顶温度均在-20℃以下。降水阶段7×7范围云顶温度先降低后上升,云顶温度梯度先上升后下降,对应积云高度先增高后降低,降水结束后2小时云顶温度逐渐恢复平衡。G_{max}峰值和半小时内G_{max}最大上升变化值ΔG_{max}均出现在强降水之前,G_{max}峰值次数为1—2次,T_{min}谷值多数出现在强降水之前也可能出现在之后,T_{min}的曲线斜率大值阶段对应G_{max}的大值阶段。ΔG_{max}和第一次G_{max}峰值G_{1max}比小时强降水结束时刻分别提前2.0—11.0 h、1.0—10.5 h,降水出现具体时间及雨强大小视降水所需的热力、动力和水汽条件的具体配置情况而定。ΔG_{max}和G_{1max}最高可达到22.3℃和48.3℃,T_{min}最低可达到-90.3℃。

(2)以7×7范围IR1和IR3通道的云顶温度极小值(x_1、x_2)、IR1通道的云顶温度梯度极大值(x_3)作为自变量,1小时降水量作为因变量,建立的降水量级预报方程,均通过了$P<0.01$的检验,能较好地模拟1小时降水量随时间的变化趋势和提前1小时预测到强降水,模拟计算值与真值相差1个降水量级。在考虑G_{max}峰值对强降水的贡献后R^2由0.23提高到0.54,模拟的降水量峰值与真值峰值明显接近。并且当云顶温度同时满足$x_1<0$℃,$x_2<-20$℃和$x_3>4$℃时,可初步作为即将有降水产生的先兆条件;当G_{max}第2次峰值大于15℃时,强降水将在3小时内产生;当$\Delta G_{max}>8$℃且$G_{1max}>15$℃时,或$G_{1max}>30$℃时,或云顶温度极小值$T_{min}<-60$℃时,满足条件之一则强降水在未来6小时内产生,可初步作为强降水发生的先兆条件。

(3)根据云顶最低温度选择云团识别阈值,同时满足最短质心距离和最大相关系数的对流云团识别和追踪方法,计算量小、准确率高。检验结果对形变较小的云团(相关系数≥0.5)的准确率为100%,对发生了合并或分裂等严重形变的云团(一般相关系数<0.5)的识别结果正确而追踪结果无效。

(4)高原东部暴雨云团均属于中-β—中-α尺度对流云团,水汽柱深厚但强度弱于低海拔地区强雷暴云团。高原东部对流云团的质心位置的IR1和IR2通道亮温差小于或等于-2 K、IR1与IR3通道亮温差小于或等于7 K、深对流指数大于或等于13,对流云团平均云顶温度小于或等于-40℃,$G_{max}\geq 11$℃,T_{min}为-40.6— -90.3℃,则属于暴雨云团。多数情况下局地暴雨开始前3小时内有对流云团覆盖测站,若对流云团空间参数(云顶最低温度、低温质心和最大温度梯度位置)靠近测站,一般最小距离小于或等于15个像距则测站将有降水或强降水产生。当最小距离小于或等于5个像距则3小时内测站一定有降水产生,多数情况有强降水产生。最小距离时刻可能比测站7×7范围的G_{max}峰值时刻提前或推后0—3 h,但均比最强小时降水结束时刻的提前0.5—3.0 h。

(5)高原东部暴雨云团产生局地强降水过程,在雷达回波图上表现为强降水超级单体风暴特征,产生雷雨、冰雹和大风天气。存在较明显的低层高反射率因子梯度和前侧入流对应的弱回波区、以及暴雨阶段的后侧下沉辐散气流。暴雨测站7×7范围的云顶温度梯度最大峰值时刻对应雷达18 dBz回波顶高度梯度极大值、IR1和IR2云顶最低温度谷值时刻对应雷达回波顶高度极大值、IR3云顶最低温度谷值时刻对应垂直累积液态水含量的极大值。

由于高原地形复杂、测站稀疏和降水分布不均,且夏季对流降水受地形影响很大等因素,能观测到降水量的暴雨云团降水过程很少且均是局地暴雨,因此统计的样本数有限,本研究结论将在今后的工作中继续改进和完善。

参考文献(References)

Adler R F and Negri A J. 1988. A satellite infrared technique to estimate tropical convective and stratiform rainfall. Journal of Applied Meteorology, 27(1): 31-51 [DOI: 10.1175/1520-0450(1988)027 <0030: ASITTE>2.0.CO;2]

Bergès J C, Jobard I and Roca R. 2009. A new index to estimate precipitation using cloud growing rate. Geophysical Research Letters, 36(8): 1-5 [DOI: 10.1029/2008GL036665]

陈佩燕,端义宏,余晖,胡春梅. 2006. 红外云顶亮温在西北太平洋热带气旋强度预报中的应用. 气象学报,64(4): 474-484

Hong Y, Kuo L H, Sorooshian S and Gao X G. 2004. Precipitation estimation from remotely sensed imagery using an artificial neural network cloud classification system. Journal of Applied Meteorology, 43

(12): 1834－1852 [DOI: 10.1175/JAM2173.1]
胡波，杜惠良，肖云. 2005. 用云团强中心附近最大亮温梯度区判别强降水. 气象科技，33(5): 401－403
胡渝宁，李森. 2012. 基于 FY2D 静止气象卫星云图中雷暴云团的识别 // 中国会议，S1 灾害天气研究与预报. 北京: 中国气象学会
江吉喜，范梅珠. 2002. 夏季青藏高原上的对流云和中尺度对流系统. 大气科学，26(2): 263－270
李森，刘健文，刘玉玲. 2010. 基于 FY2D 静止卫星云图的强对流云团识别. 气象水文海洋仪器，27(2): 72－78
Lin C C，Zhang C A，Lin Z M，Lin X M，Xie Y F and Zheng S Z. 2003. Study on the relationship between brightness temperature from GMS-5 infrared cloud imagery and surface rain rates during the raining seasons of Fujian province. Journal of Tropical Meteorology，9(1): 74－79 [DOI: 10.3969/j.issn.1006－8775.2003.01.009]
刘延安，魏鸣，高炜，李南. 2012. FY-2 红外云图中强对流云团的短时自动预报算法. 遥感学报，16(1): 79－92
卢乃锰，吴蓉璋. 1997. 强对流降水云团的云图特征分析. 应用气象学报，8(3): 269－275
Mahrooghy M，Younan N H，Anantharaj V G and Aanstoos J. 2011. High resolution satellite precipitation estimate using cluster ensemble cloud classification // Proceedings of the 2011 IEEE International Geoscience and Remote Sensing Symposium (IGARSS). Vancouver: IEEE: 2645－2648 [DOI: 10.1109/IGARSS.2011.6049746]
Mahrooghy M，Younan N H，Anantharaj V G and Aanstoos J. 2012. On the use of a cluster ensemble cloud classification technique in satellite precipitation. IEEE Journal of Selected Topics in Applied Earth Observations and Remote Sensing，5(5): 1356－1363 [DOI: 10.1109/JSTARS.2012.2201449]
滕卫平，杜惠良，胡波，俞善贤. 2006. 浙江省降水云系红外云图特征及其与降水量的关系. 气象科技，34(5): 527－531
Vicente G A，Scofield R A and Menzel W P. 1998. The operational GOES infrared rainfall estimation technique. Bulletin of the American Meteorological Society，79(9): 1883－1898 [DOI: 10.1175/1520－0477(1998)079<1883: TOGIRE>2.0.CO;2]
俞小鼎，周小刚，Lemon L. 2010. 强对流天气临近预报. 北京: 中国气象局培训中心，18－29
张驹，王敏，顾清源. 2007. 四川 2006 年"9.3"暴雨过程中 TBB 与强降水对应关系分析. 四川气象，27(2): 7－9
赵强，程路. 2009. 云顶亮温在一次区域性暴雨中的分析与应用. 陕西气象，(4): 1－4
郑世林，席世平. 2006. 河南省 2005－06－21 强对流天气分析. 河南气象，(3): 46－47
朱平，李生辰，肖建设. 2012. 青海省短时强对流天气雷达自动预警技术应用初步研究. 暴雨灾害，31(2): 182－187